UNITED NATIONS UNIVERSITY
GEOTHERMAL TRAINING PROGRAMME
Orkustofnun, Grensasvegur 9,
IS-108 Reykjavik, Iceland

Reports 2012
Number 11

JOINT 1D INVERSION OF MT AND TEM DATA FROM MENENGAI GEOTHERMAL FIELD, KENYA

Joseph M. Gichira
Geothermal Development Company, Ltd. – GDC
P.O. Box 17700 – 20100
Nakuru
KENYA
jgichira@gdc.co.ke

ABSTRACT

With an estimated geothermal potential of 10,000 MWe, Kenya has so far managed to develop slightly above 200 MWe and additional 280 MWe are on course. The Menengai volcanic system and caldera on the East African Rift is in a very strategic position for tapping geothermal energy. Understanding the resistivity structure of Menengai geothermal field should give a good understanding of the subsurface and enhance the possibility for the exploitation of this abundant geothermal resource. The subsurface was imaged using resistivity methods namely: MT and TEM. The resistivity structure of Menengai revealed four major resistivity layers. These layers are: a high-resistivity surface layer extending to a depth of about 300 m below the surface; a low-resistivity anomaly considered to be the cap-rock of the Menengai geothermal system, with a layer thickness of more than 700 m; a high-resistivity core which runs from a depth of 1600-3000 m, which is interpreted as the reservoir; and further below it, a low-resistivity zone which is interpreted to be the heat source. Temperature measurements from a well drilled to a depth of 2100 m correlated very well with the resistivity structure of Menengai.

1. INTRODUCTION

The African Rift starts in the Afar region and passes through Ethiopia and Kenya, north to south, making Kenya a potential spot for geothermal resources. Along the Kenyan rift are the various prospects identified for geothermal exploration. Amongst them is the Olkaria geothermal field (Figure 1) which is well explored and developed and in the process of expansion, while Menengai field is in the process of exploration drilling. Normally, detailed surface investigations using various exploration methods is done before a field is committed for exploration drilling and development. In geothermal exploration, various exploration techniques are employed including geophysics, geology, geochemistry and heat flow measurements. The electrical resistivity technique is the most common geophysical method used for geothermal investigation.

The Menengai geothermal field is a high-temperature field and has attracted the attention of the government, making it a major priority area for geothermal exploration and development in Kenya. The Menengai geothermal field covers the Menengai volcano, the Ol'Rongai volcanoes, Ol-Banita plains and parts of the Solai graben to the northeast. It is estimated that the total field measures approximately 850 km^2 (GDC, 2010).

Geophysical exploration techniques play a key role since they are the only means of locating deep seated structures that are controlling the geothermal system, namely heat sources and possible conduits for geothermal fluids and delineating the resource potential areas and are, therefore, very critical in determining the drilling sites. The geophysical techniques that were employed in this study of Menengai field are the Transient Electromagnetic (TEM) and Magneto Telluric (MT) resisitivity methods. The results of this investigation are presented in the form of iso-resistivity maps and cross-sections. Figure 1 is a map showing all geothermal prospect areas along the Kenyan rift with Menengai marked with a bold red arrow.

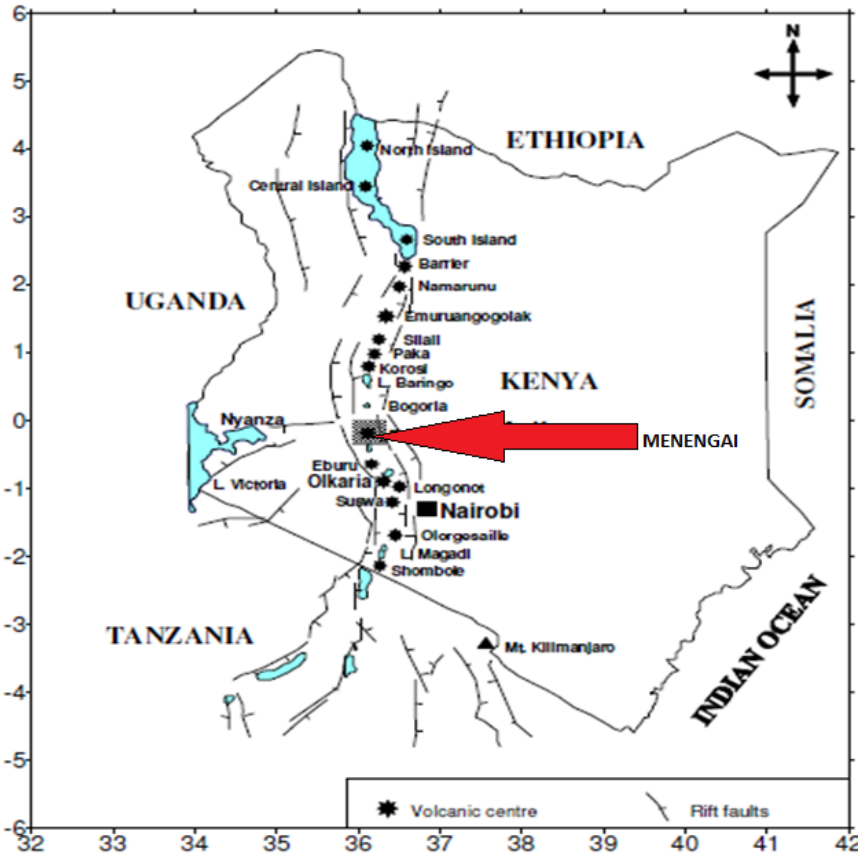

FIGURE 1: Map showing the location of Menengai geothermal prospect and other prospects along the Kenyan Rift Valley (GDC, 2010)

2. AN OVERVIEW OF THE TECTONICS, GEOLOGY AND STRUCTURES IN MENENGAI

2.1 Tectonic setting

The Kenya Rift Valley is a prominent feature of geographic and geologic interest. It is a tectonic feature that runs from Lake Turkana in Kenya in the north to Lake Natron (Tanzania) in the south. It forms a classic graben averaging 40-80 km wide (Figure 2). The Kenyan rift is part of the East African Rift system, which is an intra-continental divergence zone where rift tectonism, accompanied by intense volcanism, has taken place from the late Tertiary to the present. The rift developed within a stable orogenic belt that skirts around a craton. Several Quaternary volcanoes occur within the rift floor of the Kenya segment of the rift. Most of the volcanic centres have had one or more explosive phase(s) including caldera collapse. Some centres are dotted with hydrothermal activity and are envisaged to host geothermal systems driven by magmatic heat sources.

The Menengai geothermal prospect is located within an area characterized by complex tectonic activity associated with a rift triple junction. This is a zone at which the failed rift arm of the Nyanza rift joins the main Kenyan rift. The Kenyan rift is characterized by extension tectonism where the E-W tensional forces resulted in block faulting, which include tilted blocks as evident in both the floor and scarps of the rift. Narrow scarps that show little effect of movement and have been eroded resulting in gentle scarps characterize the western margin. The eastern margins, however, depict wider belts with sharp scarps, implying recent active movements. The rift trough is cut by numerous normal faults that clearly represent continued extensive tectonism under the rift floor. Figure 3 shows a structural map of

Menengai. Two rift floor tectono-volcanic axes (TVA) that are important in controlling the geothermal system in the study area include the Molo and the Solai TVA.

2.2 Surface geology

Figure 2 shows a simplified geological map of the Menengai area. Most of the area around the caldera is covered mainly by pyroclastics erupted from centres associated with Menengai volcano. Young lava flows infilling the main caldera are post caldera in age. Older (Pleistocene) lavas, mainly trachytic and phonolitic in composition, are exposed in the northern parts and are overlain by eruptives from Menengai volcano. Some alluvial deposits are found in low-lying narrow grabens where they are deposited as thin reworked layers. One isolated exposure of diatomaceous bed was noted on the caldera floor, probably indicative of prehistoric climates and the existence of shallow fresh lakes in this part of the rift.

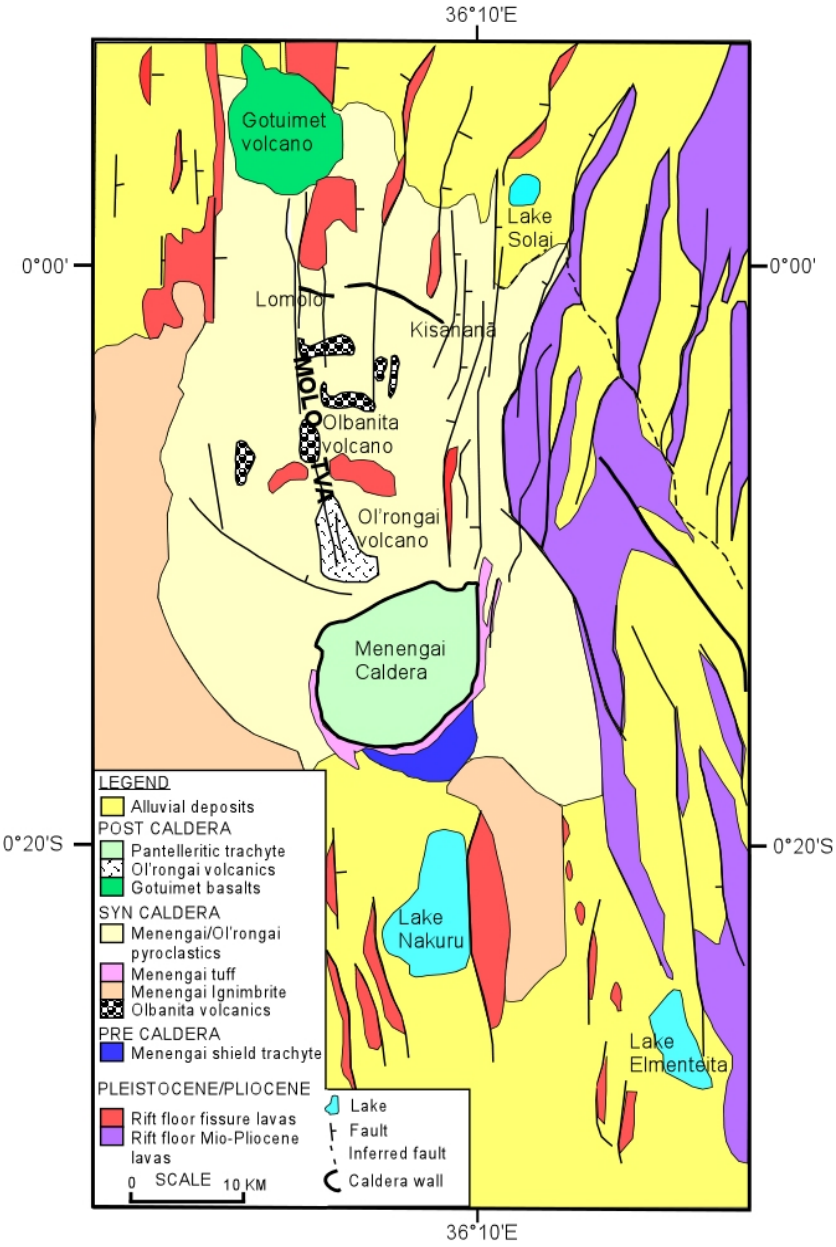

FIGURE 2: Simplified geological map of Menengai geothermal prospect showing theoutline of the caldera, volcanic centres and other structures

The area has been divided into three zones whose surface rocks depict different eruption styles for clarity of descriptions, namely: the northern zone, comprised of scarps that have exposed older lava flows; the central zone which consists of flat grounds that are covered by derivatives of plinian eruptions with a few interrupting scarps; and the Menengai volcano comprising the caldera floor. The post-caldera eruptives are mainly lavas flows infilling the Menengai caldera floor. The eruption of post caldera lavas may have been preceded by explosive episodes, suggested by the presence of ash and pumice products in the caldera floor. This eruption episode probably occurred contemporaneously both inside the caldera floor and at Ol'Rongai.

2.3 Structural geology

The structural systems are best interpreted by examining the regional tectonic map shown in Figure 3. The major structural systems in the area may be grouped into three, namely: the Menengai caldera, the MoloTectono-volcanic axis and the Solai Graben. Each of these systems is described individually below.

2.3.1 Menengai caldera

The Menengai caldera is an elliptical depression with minor and major axes measuring about 7.5 km and 11.5 km, respectively. The circular rim of the caldera ring fault is well preserved with a vertical cliff measuring up to about 400 m in some places. The ring structure has only been disturbed by the Solai graben faults on the northeast end and one fracture south-southwest of the caldera wall extending southwards (Figure 3). Other disturbances at the southeast and northwest ends may be grabens that existed before the caldera collapsed. The caldera floor is covered with post-caldera lavas such that it is not possible to estimate the collapse depth or any structures within the caldera floor. However, most of the caldera infill lavas are fissure eruptions that billowed out of the fracture openings.

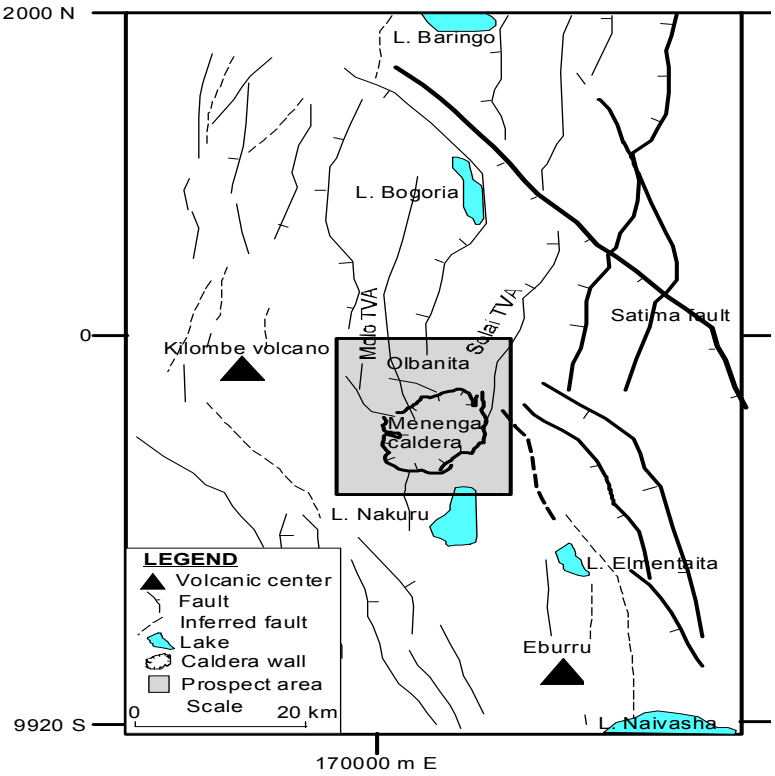

FIGURE 3: Map showing the structural set-up of the Kenyan rift floor between Lake Naivasha and Lake Baringo

2.3.2 Molo TVA/Ol'Rongai structural system

The Molo TVA (Geotermica Italiana, 1987) is a very prominent volcano-structural feature represented on the surface by a zone with a concentration of faults and fractures along which volcanic eruptions have taken place (Figure 3). This structure extends from southeast of the Lake Baringo sedimentary basin and east of Lake Bogoria where it forms a narrow (4 km wide) graben cutting through the Lake Bogoria phonolite suite far north of the prospect area. The structure can be traced past the Goitumet basaltic volcano. Arus steam jets are located on the eastern boundaries of this important TVA. The structure runs further southwards under Menengai volcanics (north of the Olbanita area) and resurfaces again in the Ol'rongai area. Volcanic eruptions issued along faults/fractures in the zone.

The Ol'rongai structural system represents a part of the larger Molo TVA that has had a lot of volcanic activity, including eruptions that resulted in a buildup of a north-northwest trending ridge referred to as Ol'rongai volcanoes. On the regional set-up, the structure extends northwards through Lomolo as far as the Goitumet volcanic centre. Over the Ol'rongai area, the structure is marked by intense volcanic activity including explosive (pumice issuing) craters. This part of the structure is adjacent to the Menengai caldera and possibly extends into the caldera.

2.3.3 Solai area

The Solai tectonic axis is a narrow (4 km wide on average) graben that runs in N-S direction from the eastern end of the Menengai caldera, through Solai. It is comprised of numerous fault/fracture systems trending N-S. The eastern boundary of the graben probably extends to the foot of the Marmanet escarpment. This is the only system that has cut the Menengai pyroclastics. On the northern end, it also cuts through the Pleistocene trachyphonolites of the Lake Bogoria suite, northwest of Kisanana out of the prospect area. Its southern extension under the Menengai volcanic pile is important as a hydrogeological control and a possible permeability enhancement of brittle lava formations underlying the Menengai eruptives.

3. RESISTIVITY OF ROCKS

Most rock forming minerals are electrical insulators in their natural state. Resistivity is controlled by the movement of charge carriers in different materials. Electrons are the charge carriers in solid rocks while ions are the charge carriers in fluids and or solutions. The concentration and mobility of charge carriers determines the resistivity of different rocks. Although water is not a good conductor of electricity, saline groundwater with elevated temperatures largely lowers the resistivity of rocks which is usually the case in geothermal areas (Figure 4). Groundwater movement is facilitated by interconnected pores and fractures, thus causing hydrothermal alteration to the rocks.

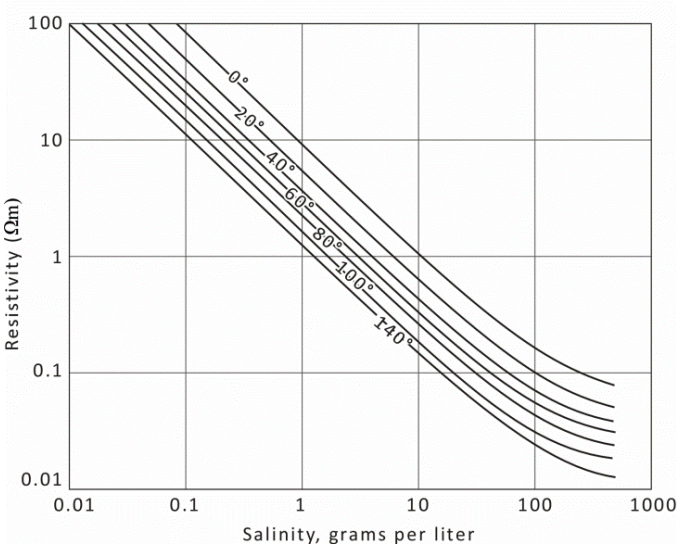

FIGURE 4: The resistivity of solutions of NaCl as a function of concentration and temperature (Keller and Frischknecht, 1966)

The resistivity of a material is defined as the resistance in ohms (Ω) between the opposite faces of a unit cube of the material (Kearey et al., 1994). For a conducting cylinder of resistance (R), length (L) and cross-sectional area (A) the specific electrical resistance (often shortened as resistivity) is given by:

$$\rho = \frac{RA}{L} \tag{1}$$

where ρ = Specific resistivity (Ωm);
R = Resistance (Ω);
A = Area (m^2)
L = Length (m)

The electrical resistivity of rocks depends on the following parameters (Hersir and Björnsson, 1991):

- Porosity and the pore structure of the rock
- Salinity of water
- Amount of water
- Water rock interaction and alteration
- Temperature
- Pressure

Understanding these physical parameters is important in geophysics as they help us in building a picture of a geothermal system. With a good knowledge of electrical resistivity, it is possible to delineate the boundaries of a geothermal resource. This information is very valuable, especially when developing conceptual models for geothermal prospects.

3.1 Porosity, permeability and the pore structure of the rock

Porosity is defined as the ratio between the pore volume and the total volume of a material, and is measured as a fraction between 0 and 1 or as a percentage between 0 and 100. Porosity is therefore a measure of a rock´s ability to hold fluids. It can be classified into three major classes, namely:

Intergranular porosity, where the pores are formed as spaces between grains or particles in a compact material like sediments and volcanic ash.

Joints-fissures or fractures, where the pores are formed by a net of fine fissures caused by tectonics or cooling and contraction of the rock (igneous rocks, lava).

Vugular porosity, where big and irregular pores have been formed due to dissolution of material, especially in limestone or gas bubbles in volcanic rocks.

The empirical Archies's law states that resistivity varies approximately as the inverse power of the porosity when a rock is fully saturated with water. An empirical function relating resistivity and porosity, known as Archie's law (Archie, 1942), is widely used:

$$\rho = \rho_w a \varphi_t^{-n} \tag{2}$$

where ρ = Bulk (measured) resistivity;
ρ_w = Resistivity of the pore fluid;
φ_t = Porosity in proportions of total volume;
a = Empirical parameter that varies from <1 for intergranular porosity to >1 for joint porosity, usually around 1;
n = Cementing factor, an empirical parameter that varies from 1.2 for unconsolidated sediments to 3.5 for crystalline rocks, usually around 2.

Archie's law is valid if the resistivity of the pore fluid is on the order of 2 Ωm or less, but doubts are raised if the resistivity is much higher (Flóvenz et al., 1985). However, Archie's law seems to be a fairly good approximation when the conductivity is dominated by the saturating fluid (Árnason et al., 2000).

Pemeability is the ability of rocks to transmit fluids. This is guided by the interconnectivity of pores, thus permeability is closely related to porosity. Pore spaces must be interconnected and filled with water if fluid conduction is to take place. The degree to which pores are interconnected is called effective porosity. The range of values for permeability in geological materials is extremely large with the most permeable materials having permeability values that are millions of times greater than the least permeable ones. In addition to the characteristics of the host material, the viscosity and pressure of the fluid also affect the rate at which the fluid will flow (Lee et al., 2006).

3.2 Salinity of water

The bulk resistivity of a rock is mainly controlled by water rock interaction and pore fluid resistivity which is dependent on the salinity of the fluid. An increase in the amount of dissolved solids in the pore fluid can increase conductivity by large amounts. Conductivity in solutions is a function of salinity and the mobility of ions present in the solution. Considering water as an electrolyte, the conductivity of an electrolyte solution can be expressed as shown in Equation 3 (Hersir and Björnsson, 1991):

$$\sigma = {}^{1}/_{\rho} = F(c_1 q_1 m_1 + c_2 q_2 m_2 \ + \cdots) \quad (3)$$

where σ = Conductivity (S/m);
F = Faradays number (9.65×10^4 C/mole);
c_i = Concentration of ions (mole);
q_i = Valence of ions; and
m_i = Mobility of ions (m^2/Vs)

3.3 Temperature

The resisitivity of aqueous solutions has been observed to decrease with increasing temperature due to an increase in ion mobility caused by a decrease in the viscosity of the water. This is usually evident at moderate temperatures between 0 and 200°C. This can be expressed using the Dakhnov relationship (Dakhnov, 1962) as:

$$\rho_w = \frac{\rho_{wo}}{1 + \alpha(T - T_0)} \quad (4)$$

where ρ_w = Resistivity of the fluid at temperature T (Ωm);
ρ_{wo} = Resistivity of the fluid at temperature T_0 (Ωm);
α = Temperature coefficient of resistivity, $\alpha \approx 0.023°C^{-1}$;
T_0 = Room temperature (23°C).

At high temperatures, there is a decrease in the dielectric permittivity of the water, resulting in a decrease in the number of dissociated ions in the solution causing an increase in the fluid resistivity. At temperatures above 300°C, fluid resistivity starts to increase. This is summarized in Figure 5 by Hersir and Björnsson (1991).

3.4 Water rock interaction and alteration mineralogy

Hydrothermal water reacts with rocks to form alteration minerals through a process called hydrothermal alteration. The distribution of alteration minerals in the subsurface gives information on the temperature of the geothermal system and the hydrothermal water flow paths. The alteration intensity is lower near the surface, where the temperatures are low, and higher deep in the subsurface where the temperatures are high. The resistivity structure of high-temperature geothermal systems in the world hosted in volcanic rocks shows similarity such as in Icelandic and Kenyan geothermal fields. The degree of alteration varies depending on the rock types, fluid chemistry, porosity and permeability of the rocks.

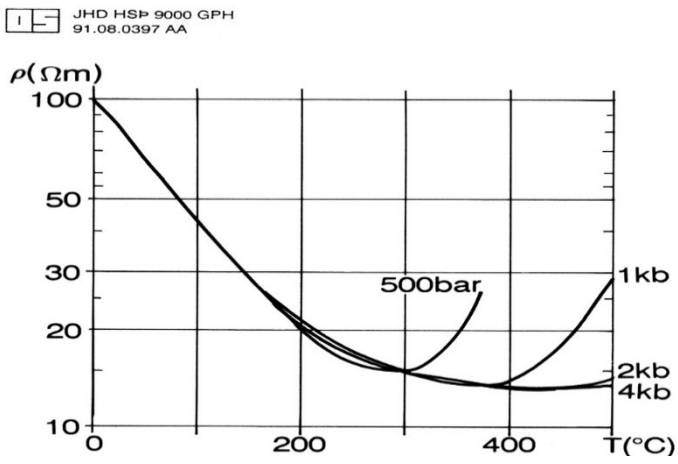

FIGURE 5: Electrical resistivity of solutions of NaCl water as a function of temperature at different pressures (Hersir and Bjornsson, 1991)

Figure 6 shows a summary of the resistivity and alteration mineralogy in a high-temperature system. The uppermost and unaltered part has relatively high resistivity and the conduction is mainly pore fluid conduction. The resistivity decreases as the smectite-zeolite zone is reached and mineral or surface

conduction becomes the dominant conduction mechanism. Because of increasing temperature and increasing alteration at greater depth, the resistivity decreases even further. Below, the mixed clay zone becomes dominant and the resistivity increases again, most likely due to the strongly reduced cation exchange capacity of the clay minerals in the mixed clay and chlorite zone. Here the surface and pore fluid conduction probably dominates as the mineral conduction is diminished. The transition from smectite to mixed-layer clay happens at a temperature of around 230-250°C. At about 250-300°C, the smectites disappear and the mineral chlorite dominates this zone. At even higher temperatures epidotes appear and dominate, marking the start of the high-temperature zone which is usually resistive. The high resistivity at this point is brought about by the crystalline nature of the mineral epidote; thus the anion and cation exchange is reduced. The conduction mechanism here is mainly surface and pore fluid.

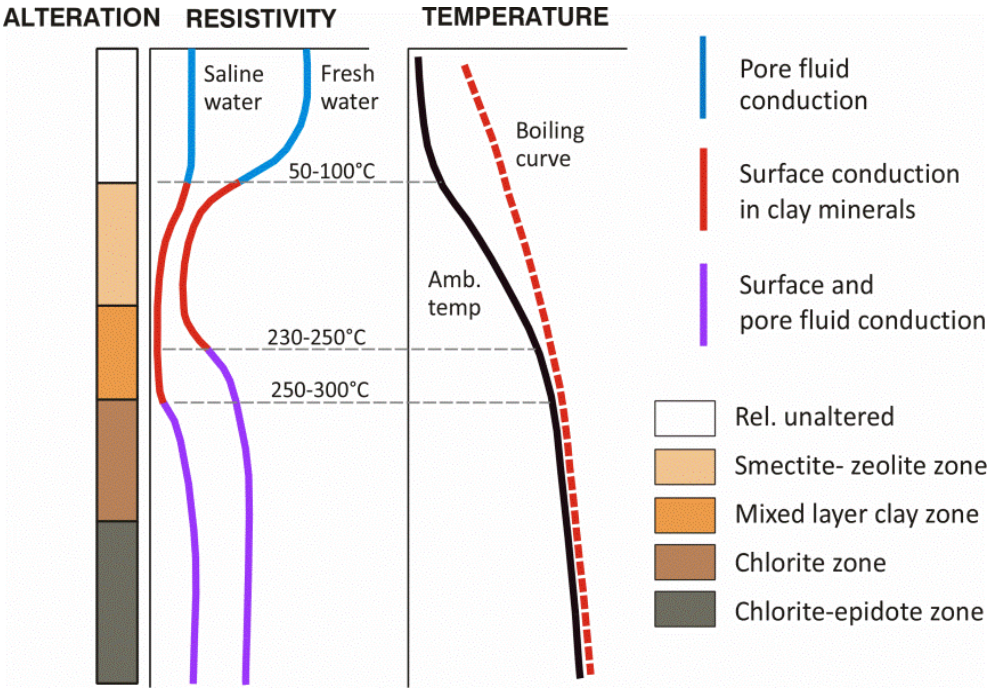

FIGURE 6: The general resistivity structure of a high-temperature geothermal system showing resistivity variations with alteration and temperature (Flóvenz et al., 2005)

4. OVERVIEW OF GEOPHYSICAL METHODS

4.1 Structural methods

Structural methods give information about geological structures rather than parameters directly associated with hydrothermal systems.

Magnetic surveys. In geothermal exploration, magnetic surveys are employed mainly for mapping geological structures. The most important applications are finding the depth and the location of concealed intrusives, locating dykes and faults, finding the depth to the basement, evaluating paleomagnetism and locating hydrothermally-altered areas.

Gravity surveys (Hersir and Björnsson, 1991). In geothermal exploration, the gravity method is used to detect geological formations and lateral density variations. Different types of rocks in the subsurface have different densities, hence different gravitational forces. The gravity force between two masses, m_1

and m_2, at a distance r apart, is given by Newton's law of gravitation (m_1 is the first mass and m_2 is the mass of the earth):

$$F = G\frac{m_1 m_2}{r^2} \quad (5)$$

where G = The universal gravitational constant, $G = 6.670 \times 10^{-11}$ Nm^2/kg^2.

Gravity variations are measured with a gravimeter. These are very sensitive mechanical instruments which measure the change in acceleration (g) at one place relative to another reference place (relative measurement). The unity for acceleration is m/s^2. A gravity unit (g.u.) is equal to 10^{-6} m/s^2. One g.u. is equal to 0.1 mgal. The sensitivity of gravimeters is about 0.005 mgal. Absolute gravimeters are now being developed. They are already used in the field to measure gravity at selected base stations. Their accuracy is similar to the accuracy of conventional gravimeters. In order to obtain information about the subsurface density from gravity measurements, it is necessary to make several corrections to the measured gravity values before they can be represented in terms of geological structures. The final corrected value for the gravity anomaly is called the Bouguer anomaly, Δg_B. It can be expressed as:

$$\Delta g_B = g_M + C_{FA} - C_B + C_T - g_N \quad (6)$$

where g_M = Measured gravity corrected for tidal effects and drift in the gravimeter;
C_{FA} = Elevation correction or free-air correction;
C_B = Correction for excess mass material between the station and sea level;
C_T = Topographical correction for local terrain variations near the station;
g_N = Normal reference gravity; it takes into account the latitude of the station.

Seismic surveys. Active seismic measurements involve injecting sound waves into the ground and recording the energy that reflects or refracts back at different times and locations on the surface using geophone receivers. Processed seismic data can give information about subsurface geology, including sound velocity, rock types and fault structures. It can also be correlated with gravity to define more accurate velocity and density models which provide more accurate depth estimates, useful while developing conceptual models and eventually locating drilling sites. The passive seismic method makes use of naturally induced micro-earthquake activities and can be used to delineate permeable fractures acting as a flow path for geothermal fluids, delineate the brittle-ductile zone, and also to monitor useful indicators in natural or induced changes in the reservoir during exploitation of a geothermal field (see Simiyu et al., 1998).

4.2 Direct methods

Thermal methods directly measure temperature and heat flow (temperature surveys). No other methods have such a good correspondence with the properties of the geothermal system. There are approximately four sub-categories:

- Temperature alone (direct interpretation, mapping);
- Geothermal gradient (vertical variation of temperature measured in soil or drill holes);
- Heat flow (calculated from the product of gradient and thermal conductivity); and
- Heat budgets (measuring spring flow and steam output and/or integrating heat flow).

Measuring the temperature alone, or the geothermal gradient, is of direct significance in local geothermal work, while measuring the heat flow is of more regional or global interest. Heat can be exchanged in different ways such as by conduction (transfer of heat through a material by atomic vibration; convection (transfer of heat by motion of mass, i.e. liquid, natural circulation of hot water); and through radiation (does not play any significant role in geothermal exploration). Conduction plays a significant role in the transfer of heat in the earth's crust. Thermal convection is usually a much more effective heat

transfer mechanism than thermal conduction and is most important in geothermal systems (Hersir and Björnsson, 1991).

Electrical resistivity methods: Measuring the electrical resistivity of the subsurface is the most powerful prospecting method in surface geothermal exploration. Resistivity is directly related to the properties of interest, like salinity, temperature, porosity (permeability) and alteration mineralogy. To a great extent, these parameters characterise a reservoir (Hersir and Björnsson, 1991). Resistivity, ρ, is defined through Ohm's law, which states that the electrical field strength, E (V/m) at a point in a material is proportional to the current density, J (A/m^2):

$$E = \rho J \tag{7}$$

The proportional constant, ρ, depends on the material and is called the (specific) resistivity and is measured in Ωm. The reciprocal value of resistivity is conductivity ($1/\rho = \sigma$). There exists a variety of resistivity methods. Here we give a broad overview of the most common methods that have been used in geothermal exploration. The most important ones (electromagnetic methods) are discussed in more detail in the next chapter.

DC methods: These are active methods where a constant current, I (independent of time), is introduced into the ground through a pair of electrodes on the surface of the earth. The current creates a potential field in the earth. By measuring the electrical field, E (potential difference over a short interval), the subsurface resistivity can be inferred. Two types of DC methods have been commonly used namely: resistivity sounding, resistivity profiling.

In *resistivity sounding* resistivity is mapped as a function of depth. Measurements are made at a specified fixed central point for different distances between the electrodes. This method is used to measure variations in resistivity with depth; an example of this is the Schlumberger method.

In *resistivity profiling*, resistivity is measured mapped laterally, with the electrode arrangement at fixed distances and measurements are made as the entire array is moved along a profile. It is designed to locate lateral variations in resistivity. An example of this method is head-on profiling.

Self potential (SP) is a passive method that employs measurements of naturally occurring potentials.

In *magnetotellurics (MT)* and *audio-magnetotellurics (AMT)*, fluctuations in the natural magnetic field of the earth and the induced electric field are measured. Their ratio is used to determine the apparent resistivity.

The time domain or transient electromagnetic method (TEM) is a method where a magnetic field is built up by transmitting a constant current into a loop or grounded dipole; then the current is turned off and the transient decay of the magnetic field is measured.

The common principle of all resistivity methods is to induce an electrical current into the earth and monitor signals, normally at the surface, generated by the current distribution. In conventional direct current soundings such as Schlumberger soundings, this is done by injecting current into the ground through electrodes at the surface; the signal measured is the electric field (the potential difference over a short distance) generated at the surface. In magnetotellurics (MT), the current in the ground is induced by time variations in the earth's magnetic field and the signal measured is the electric field at the surface. In transient electromagnetics (TEM), the current is also induced by a time varying magnetic field but, in this case, the source is of a controlled magnitude, generated by the current in a loop or grounded dipole and the monitored signal is the decaying magnetic field at the surface (Hersir and Björnsson, 1991).

5. ELECTROMAGNETIC METHODS

Electromagnetic techniques have proven to be very useful geophysical tools in geothermal investigations. This is due to the fact that the spatial distribution of conductivity in geothermal regions is not only determined by the host rock distribution, but is directly related to the distribution of the actual exploration target, hot water (Berktold, 1983).

5.1 Transient electromagnetic method (TEM)

The TEM method involves transmitting a constant current through a loop of wire, thereby building a constant magnetic field of known strength (Figure 7). The process of abruptly turning off the transmitter current induces, in accordance with Faraday's law, a short duration voltage pulse in the ground, which causes a loop of current to flow in the immediate vicinity of the transmitter wire (Figure 8). Immediately after the transmitter's current is turned off, the current loop can be thought of as an image in the ground of the transmitter loop (see Figure 7). However, due to ohmic heat loss in the ground, the amplitude of the current starts to decay immediately. This decaying current similarly induces a voltage that causes more current to flow, but now at a larger distance from the transmitter loop, and also at greater depth. This deeper current flow also decays due to the limited resistivity of the ground, inducing even deeper current flow and so on.

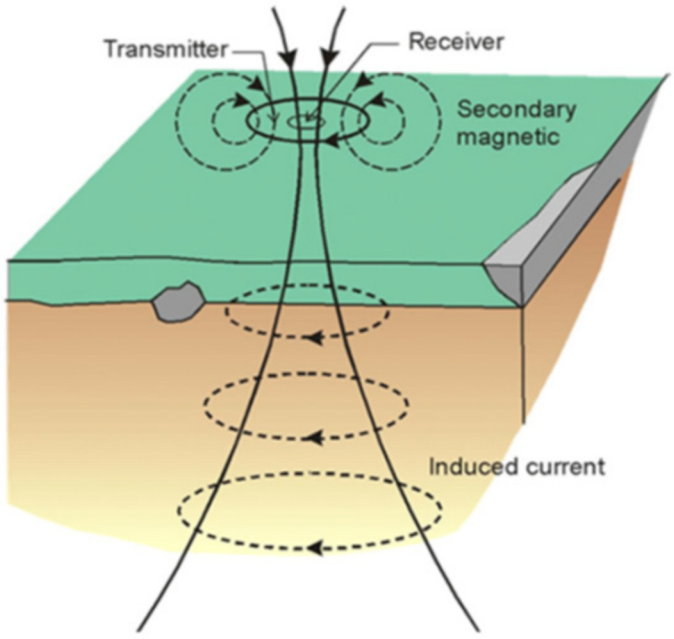

FIGURE 7: The central loop TEM configuration showing transient current flow in the ground (Hersir and Björnsson, 1991)

The depth of penetration in the central loop TEM-sounding is dependent on how long the induction in the receiver coil can be traced before it is drowned in noise. At late times, the induced voltage in the receiving coil in a homogeneous half space of conductivity, σ is (Árnason, 1989):

$$V(t,r) \approx I_0 \frac{C(\mu_0 \sigma r^2)^{\frac{3}{2}}}{10\pi^{\frac{1}{2}} t^{\frac{5}{2}}} \quad (8)$$

where $C = A_r n_r A_s n_s \frac{\mu_0}{2\pi r^3}$;

t = Time elapsed after the transmitter current is turned off (s);
A_r = Cross-sectional area of the receiver loop (m^2);
A_s = Cross-sectional area of the transmitter loop (m^2);
n_r = Number of windings in the receiver loop;
n_s = Number of windings in the transmitter loop;
μ_0 = Magnetic permeability (H/m);
I_0 = Current in the transmitter loop (A);
r = Radius of the transmitter loop (m);
$V(t, r)$ = Transient voltage (V).

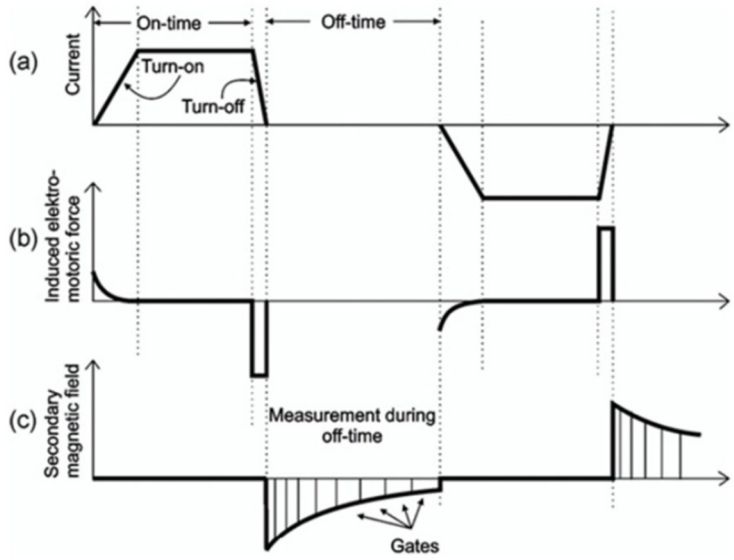

FIGURE 8: Basic principles of the TEM method: (a) Current in the transmitter loop; (b) Induced electromotive force in the ground; (c) Induction measured in the receiver coil (Christensen et al., 2006)

This shows that the transient voltage for late times, after the current in the transmitter loop is abruptly turned off, is proportional to $\sigma^{3/2}$ and falls off with time as $t^{-5/2}$. This leads to the definition of the late time apparent resistivity by solving for the resistivity in Equation 8, leading to Equation 9:

$$\rho_a = \frac{\mu_0}{4\pi}\left[\frac{2I_0\mu_0 A_r A_s n_r n_s}{5t^{5/2}v(t,r)}\right]^{2/3} \tag{9}$$

5.2 Magnetotelluric method (MT)

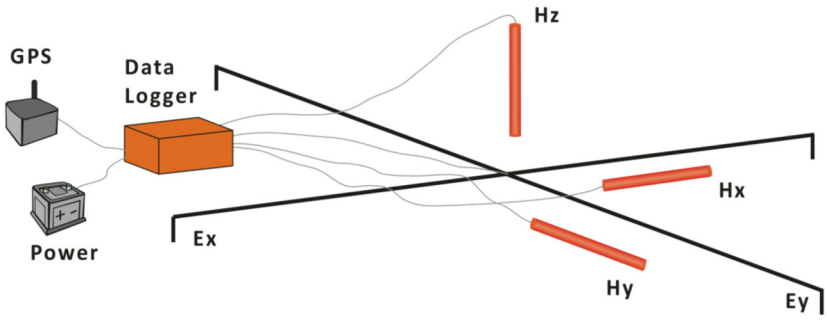

FIGURE 9: The field setup of MT soundings: Ex and Ey are the two orthogonal electric fields while Hx and Hy are magnetic channels; the Hz channel is used for strike analysis (Flóvenz et al., 2012)

MT is a passive electromagnetic geophysical method used to probe the subsurface resistivity structure. Natural variations in the earth's magnetic field induce electric currents (or telluric currents) in the ground, which depend on the earth's resistivity. Both magnetic and electric fields are measured on the earth's surface in two orthogonal directions (Figure 9).

The orthogonal electric and magnetic fields are related through the impedance tensor which holds information about the subsurface conductivity. The high frequencies give information about the resistivity at shallow depths while the low frequencies provide information about the deeper lying structures. Low frequencies (<1 Hz) have their source from the ionospheric and magnetospheric currents caused by the solar wind (plasma) interfering with the earth's magnetic field (Figure 10), while the high frequencies (>1 Hz) originate from lightning discharges near the equator. These two natural phenomena create the MT source signals over the entire frequency spectrum, generally 10 kHz to a period of some thousand seconds.

The MT method can explore resistivity down to tens or even hundreds of kilometres, which makes it the EM method which has the most exploration depth of all the EM methods, and is practically the only method for studying resistivity deeper than a few kilometres. The depth of penetration of electromagnetic fields within the earth depends on the period and the earth's conductivity structure.

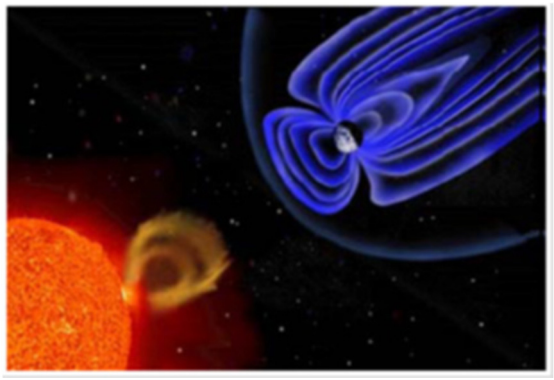

FIGURE 10: Interaction of solar wind with the magnetosphere, the source region for low frequency (< 1 Hz) natural EM fields (taken from Encyclopaedia Britannica, 2010)

The propagation of EM fields is described by the following set of relationships, called Maxwell's equations, which hold true for all frequencies:

Faraday's law:

$$\nabla \times E = -\mu \frac{\partial H}{\partial t} \tag{10}$$

Ampere's law:

$$\nabla \times H = J + \varepsilon \frac{\partial E}{\partial t} \tag{11}$$

where E = Electrical field intensity (V/m);
H = Magnetic field intensity (A/m);
J = Electrical current density, and $J = \sigma E$;
σ = Conductivity (S/m); $\rho = 1/\sigma$ (Ωm);
ε = Electrical permittivity (F/m);
μ = Magnetic permeability (H/m).

5.2.1 Electromagnetic induction in a homogeneous earth

The ratio of orthogonal components of electric and magnetic field intensity is a characteristic measure of electromagnetic properties, often called the characteristic impedance.

$$Z_{xy} = \frac{E_x}{H_y} = \frac{-i\omega\mu_0}{k} \tag{12}$$

$$Z_{yx} = \frac{E_y}{H_x} = \frac{i\omega\mu_0}{k} \tag{13}$$

where Z_{xy}, Z_{yx} = Characteristic impedance in x and y directions;
ω = Angular frequency ($2\pi f$) where f is frequency (Hz);
μ_0 = Magnetic permeability (H/m);
$E_{x,y}$ = Electric field intensity (V/m) in x, y direction;
$H_{x,y}$ = Magnetic field intensity (T) in x, y direction;
k = $\sqrt{i\omega\mu(i\omega\varepsilon + \sigma)}$ stands for the two wave propagation constant;
σ = Electric conductivity (S/m);
ε = Dielectric permittivity (Fm).

For frequencies and conductivities considered in MT the term $\omega\varepsilon$ in wave propagation constant k is much smaller than the conductivity σ and can be ignored, therefore, $k = \sqrt{i\omega\sigma}$. Putting this into Equations 12 and 13 gives:

$$Z_{xy} = \frac{E_x}{H_y} = \frac{i\omega\mu}{k} \approx \frac{i\omega\mu}{\sqrt{i\omega\sigma}} = \sqrt{i}\sqrt{\omega\rho\mu} = \sqrt{\omega\mu\rho}.\, e^{i\pi/4} \tag{14}$$

$$Z_{yx} = \frac{E_y}{H_x} = \frac{i\omega\mu}{k} = -Z_{xy} \tag{15}$$

The phase angle, θ, by which H_y lags E_x is $\pi/4$, is shown in Figure 11. If the earth is homogeneous and isotropic, then the true resistivity of the earth is related to the characteristic impedance through the following relationship (e.g. Hermance, 1973):

$$\rho = \frac{1}{\omega\mu}\left|Z_{xy}\right|^2 = \frac{1}{\omega\mu}\left|Z_{yx}\right|^2 \tag{16}$$

For a non-homogenous earth, the apparent resistivity (ρ_a) can be defined as if the earth were homogeneous using this same formula. In practical units for a homogeneous earth, the resistivity, ρ, in Equation 16 can be written as:

$$\rho = 0.2T|Z|^2 = 0.2T\left|\frac{E_x}{B_y}\right|^2 \; and \; \theta = \arg(Z) = 45° \tag{17}$$

where E' = The electrical field (mV/km);
B' = The magnetic field (nT).

Figure 11 shows the phase difference between the *E* and *H* fields for a homogenous earth.

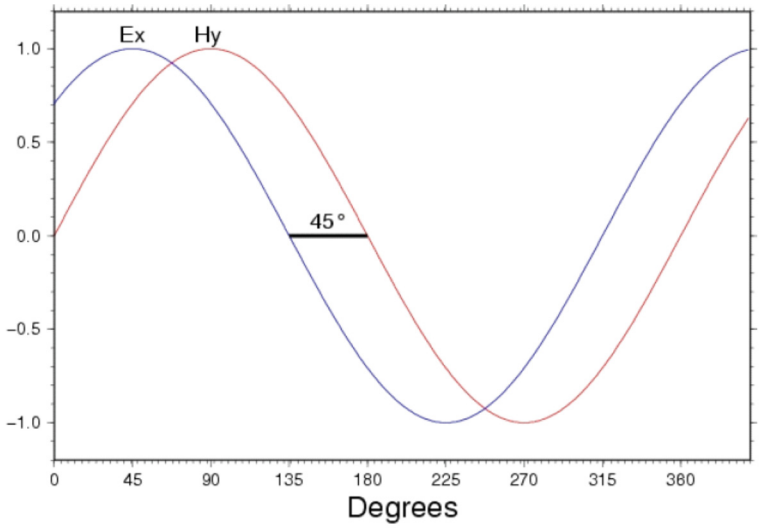

FIGURE 11: Homogenous half space response of electrical field and magnetic field describing the 45° phase difference of the E and H fields

For a non-homogeneous earth, the apparent resistivity (ρ_a) and phase (θ_a) are functions of frequency and are defined as follows:

$$\rho_a = 0.2T|Z|^2 \; and \; \theta = \arg(Z) \neq 45° \tag{18}$$

The impedance tensors

1D impedance tensor: For a 1D layered earth, the conductivity σ (or resistivity $\rho = 1/\sigma$) changes only with depth. In this case, the impedance tensor, $\boldsymbol{Z}$, may be written as:

$$Z_{1D} = \begin{bmatrix} 0 & Z_{xy} \\ -Z_{xy} & 0 \end{bmatrix} \tag{19}$$

For a layered earth, the apparent resistivity ρ_a and phase are defined as:

$$\rho_a(\omega) = \frac{1}{\omega\mu_0}|Z(\omega)|^2 \; and = tan^{-1}\left(\frac{ImZ}{ReZ}\right) \tag{20}$$

2D impedance tensor: For a 2D earth, the conductivity, σ, changes with depth and in one lateral direction. The other horizontal direction has no variation in conductivity and is commonly known as the electromagnetic or electrical strike direction. For nearly 2D earth, the strike direction can be found by rotating the coordinate system to the direction minimizing the diagonal elements of the tensor *Zxx* and *Zyy*. However, there is a 90° ambiguity in the geoelectric strike. Measuring Hz and calculating the Tipper strike resolves this ambiguity. Tipper is a parameter used for directional analysis by relating the vertical component of the magnetic field to its horizontal components. The strike is a function of frequency and is, therefore, different for different depths. In Berdichevsky and Dmitriev (2002), it is shown by decomposing the *E* and *H* into normal and anomalous field components, that in a general 2D earth, the impedance tensor becomes:

$$Z_{2D} = \begin{bmatrix} Z_{xx} & Z_{xy} \\ Z_{yx} & Z_{yy} \end{bmatrix} \tag{21}$$

Here, neither of the horizontal axes is aligned along the electromagnetic strike. In the impedance tensor, the diagonal elements *Zxx* = -*Zyy* are equal in amplitude but opposite in signs. The off diagonal elements *Zxy* and *Zyx* are independent values. However, if the impedance tensor is rotated such that the x direction is parallel and the y direction is perpendicular to the electromagnetic strike direction, the Z_{2D} impedance tensor simplifies to:

$$Z_{2D} = \begin{bmatrix} 0 & Z_{xy} \\ Z_{yx} & 0 \end{bmatrix} \tag{22}$$

The modes of the impedance tensor can be analysed independently. Transverse Electric (TE) mode or E-polarization is when the electric field is parallel to the electromagnetic strike; and Transverse Magnetic (TM) mode or B-polarization is when the magnetic field is parallel to the electromagnetic strike. In Equation 22, the TE mode is $Z_{TE} = Zxy$ and the TM mode is $Z_{TM} = Zyx$. Apparent resistivity can be calculated for each of the modes such that:

$$\rho_{a_{TE}}(\omega) = \frac{1}{\omega\mu_0}|Z_{TE}(\omega)|^2 \text{ and } \rho_{a_{TM}}(\omega) = \frac{1}{\omega\mu_0}|Z_{TM}(\omega)|^2 \tag{23}$$

3D impedance tensor: In a 3D earth, the conductivity, σ varies in all directions, σ (*x, y, z*). The impedance tensor takes the general form:

$$Z_{3D} = \begin{bmatrix} Z_{xx} & Z_{xy} \\ Z_{yx} & Z_{yy} \end{bmatrix} \tag{24}$$

All the elements in the impedance tensor in the above equation are non-zero, irrespective of rotation. There is no direction where the diagonal elements of the impedance tensor vanish, so all the elements in the tensor need to be considered.

5.2.2 Skin depth

The electromagnetic vawes that are refracted into the earth are attenuated. How fast they attenuate depends, however, on the frequency. The skin depth, δ, is the depth where the electromagnetic fields have been reduced to e^{-1} of their original value at the surface. For an oscillating electromagnetic field with time dependence *H, E*~ $e^{i\omega t}$ and for a vertically incident plane wave, the skindepth is given by:

$$\delta = 500\sqrt{T\rho}\ (m) \tag{25}$$

where δ = Skin depth (m);
T = $2\pi/\omega$ = Period (s); and
ρ = Resistivity (Ωm).

Therefore, skin depth is used as a scale length for the time-varying field, or an estimate of how deep such a wave penetrates into the earth. The formula shows that for constant resistivity, the depth of probing increases when the period T increases, and decreases when the period T decreases. Likevise, for constant period the skin depth increases with increasing resistivity.

6. MENENGAI RESISTIVITY SURVEY AND DATA PROCESSING

6.1 TEM data acquisition and processing

TEM data was acquired using two measuring instruments from different manufacturers: a ZongeGDP-32, and Phoenix V8 TEM systems. The Zonge TEM was employed in easily accessible and clear areas within the study area due to its bulkiness and used 300 m × 300 m square loop sources while the Phoenix TEM was employed in tough terrains due its portability and used 200 m × 200 m square loop sources. To investigate this response at various depths, measurements were made at frequencies of 32, 16, 8 and 4 Hertz for the Zonge and 25 and 5 Hertz for the Phoenix. A total of 120 TEM soundings have been carried out in Menengai but only 90 soundings were used for the purpose of this report (Figure 12).

The raw TEM data was processed by the program TemxZ for Zonge TEM and TemxV for the Phoenix TEM. These programs average data acquired at the same frequency and calculate late time apparent resistivity as a function of time after the current turn-off. They also enable visual editing of raw data to remove outliers and unreliable data points before the data is being used for interpretation.

6.2 MT data acquisition and processing

The data was acquired using a 5-channel MT data acquisition system (MTU-5A) from Phoenix Geophysics. The instrumentation consisted of a data recorder, induction coils, non-polarizing electrodes, Global Positioning System (GPS), 12 V battery, flash memory for data recording, and telluric and magnetic cables. The layout is such that the electric dipoles are aligned in magnetic North-South and East-West, respectively, with corresponding magnetic sensors in orthogonal directions; the third magnetic coil is positioned vertically in the ground as demonstrated in Figure 9. Before data acquisition, a start-up file is prepared with parameters like gains, filters, time for data acquisition and calibrations for both equipment and the coils and stored on a flash disk in the equipment. The ground contact resistance is generally measured to gauge the electrode coupling to the ground.

An anti-aliasing low-pass filter is used as well as a high-pass filter with a corner frequency of 0.005 Hz to remove the effect of self potential from the electric dipoles. The electric field was measured by lead chloride porous pots and the magnetic sensors were buried about 20 cm below the surface to minimize the wind effect.

In Menengai field, MT was deployed with the intention of probing to greater depths; thus, the acquiring system was left overnight so as to collect data for long periods of 20 hours or more and also to take advantage of the stronger signals usually available in the late hours of the night. This helped in getting the low-frequency signals, so we were able to achieve the objective of deep probing; the lower the frequency, the greater the depth of investigation possible at a given site. Over 200 MT soundings were carried out in this field but only 90 soundings were considered for this particular report (Figure 12).

Time-series data from the MT equipment were processed by the SSMT2000 program, provided by the equipment manufacturer, Phoenix Geophysics of Canada. First the parameter file was edited to reflect the data acquisition setup and then the resulting time-series data were Fourier transformed to the frequency domain. From the Fourier transform band averaged cross-powers and auto-powers were calculated using the robust processing method. The cross-powers were then graphically edited by the

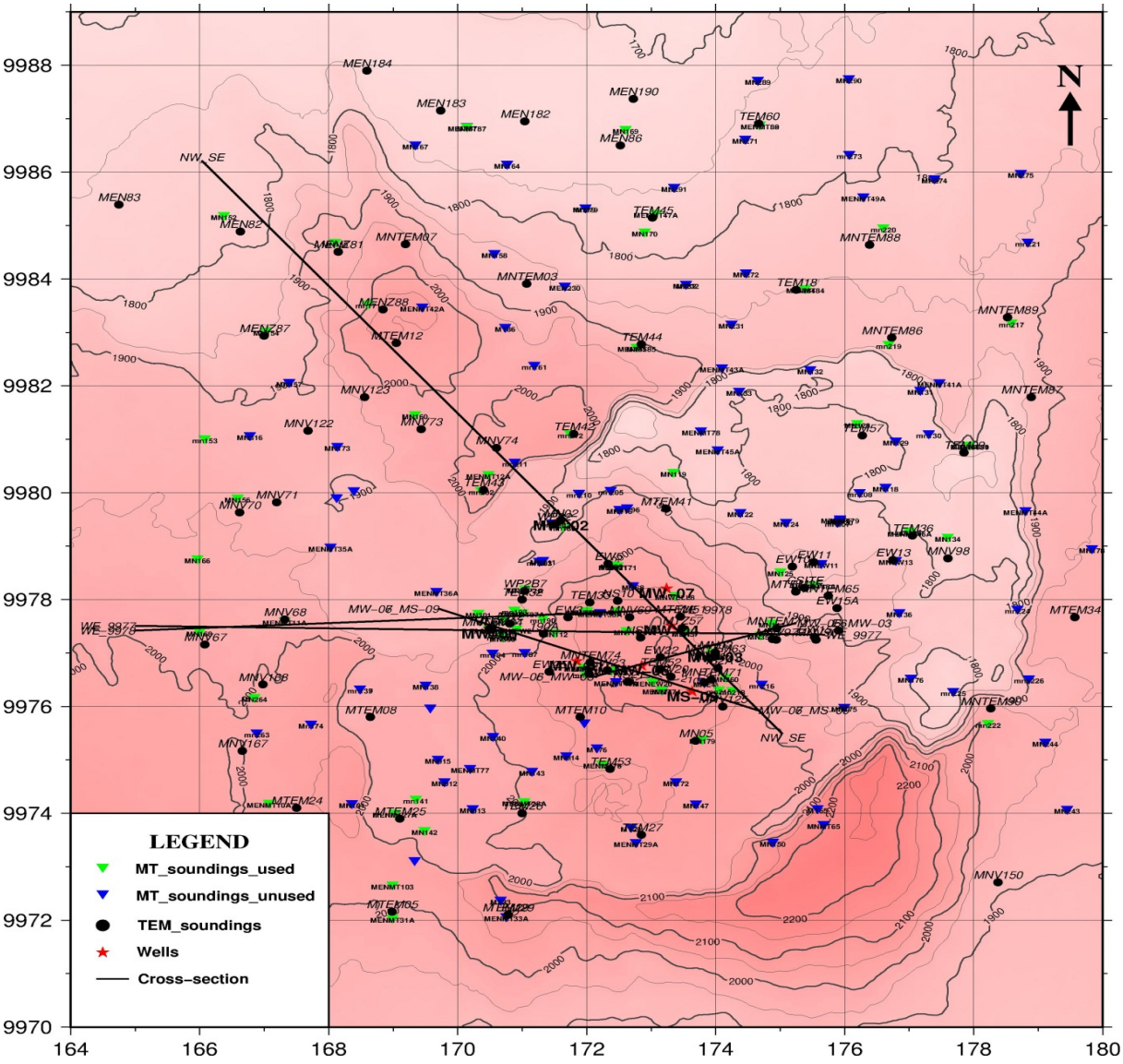

FIGURE 12: TEM and MT location map. Both green (grey) and blue (light grey) inverted triangles represent MT soundings while black circles are TEM. Red (dark) stars represent well locations while the black continuous lines denotes the cross-sections

MT editor program to remove the noisy data points and evaluate "smooth" curves for both phase and apparent resistivity. The final cross-powers and auto-powers, as well as all relevant MT parameters calculated, were stored in Electronic Data Interchange (EDI) files which are the industry's standard. These EDI files were then used as input for the Linux program TEMTD where they were used for joint inversion with the TEM.

7. DATA INVERSION

Data inversion is done to determine the relevant physical parameters that characterize a system from the measured response and it is a probability approach to the measured data. The first step in solving the inverse problem is to know how to calculate the forward problem. The first approach is to make a guess model and let the forward algorithm calculate the response and try to make the best fit with the measured

data. If the calculated response does not fit with the measured data, an inversion algorithm improves the model-based model in order to get better matches with the measured data.

Forward modelling is of central importance in any inversion method and, hence, must be fast, accurate and reliable. Inversion uses forward modelling to compute the sensitivity matrix and responses for calculating the misfit. The most commonly used inversion method for geoelectric soundings is the least-squares inversion method. After every iteration step we get a sensitivity matrix which places us near the exact model; this is characterized by the reduction in chi-square (χ).

7.1 TEM inversion

The 1D inversion of TEM was done using software called TEMTD, a UNIX program (developed at Icelandic Geosurvey by Knutur Árnason). This software models the square source loop that the receiver coil/loop is at the centre of the source loop. The current waveform is also modelled in details with exponential gurrent turn-on and linear ramped turn off. The transient response is calculated both as induced voltage and late time apparent resistivity as a function of time. The inversion algorithm used in this program is the non-linear, damped, least-squares inversion (Árnason, 2006a). The misfit function is the root-mean-square difference between measured and calculated values (chisq), weighted by the standard deviation of the measured values. In this study, the measured voltages were chosen for inversion.

The programme can do both standard layered inversion (inverting resistivity values and layer thicknesses) and Occam's inversion with exponentially increasing layer thicknesses with depth. It offers a user specified damping of the first (sharp steps) and second order derivatives (oscillations) of model parameters (logarithm of resistivity and layer thicknesses) (Árnason, 2006b).

All the TEM soundings were interpreted by 1-D inversion. The inversion was done by the Occam inversion. In 1-D inversion, it is assumed that the earth consists of horizontal layers with different resistivity and thicknesses. The 1-D interpretation seeks to determine the layered model where the response best fits the measured responses. When interpreting TEM resistivity it must be born in mind that the depth of exploration of the TEM soundings is much greater in a resistive earth than in conductive environments. This is because the fields attenuate at much shallower depth in conductive materials than in a resistive ones (Lichoro, 2009).

7.2 1D joint inversion of the TEM and MT data

The TEMTD program does 1-D inversion of TEM and MT data separately or jointly. In this study the software was used to invert MT apparent resistivity and phase derived from the rotationally invariant determinant of the MT tensor elements. In the joint inversion, one additional parameter is also inverted for, namely a static shift multiplier needed to fit both the TEM and MT data with the response of the same model. An example of a 1-D joint inversion of MT and TEM data is shown in Figure 13, where the red (dark) diamonds are measured TEM apparent resistivities and the blue (gray) squares are the MT apparent resistivities and phase.

Solid lines show the response of the resistivity model, shown to the right. The shift multiplier is shown in the upper right hand corner of the apparent resistivity plot. The TEM data has been converted from the time scale to the period scale according the the method suggested by Sternberg et al. (1988). For MT sites without an onsite TEM sounding, the closest TEM site was used for static shift correction; in this case, the TEM sites found acceptable were within a radius of 500 m. The inversion results are shown by selected cross-sections and iso-resistivity maps in the results and discussions chapter. A complete set of all the inversion results of each sounding is shown in a special appendix report (Gichira, 2012).

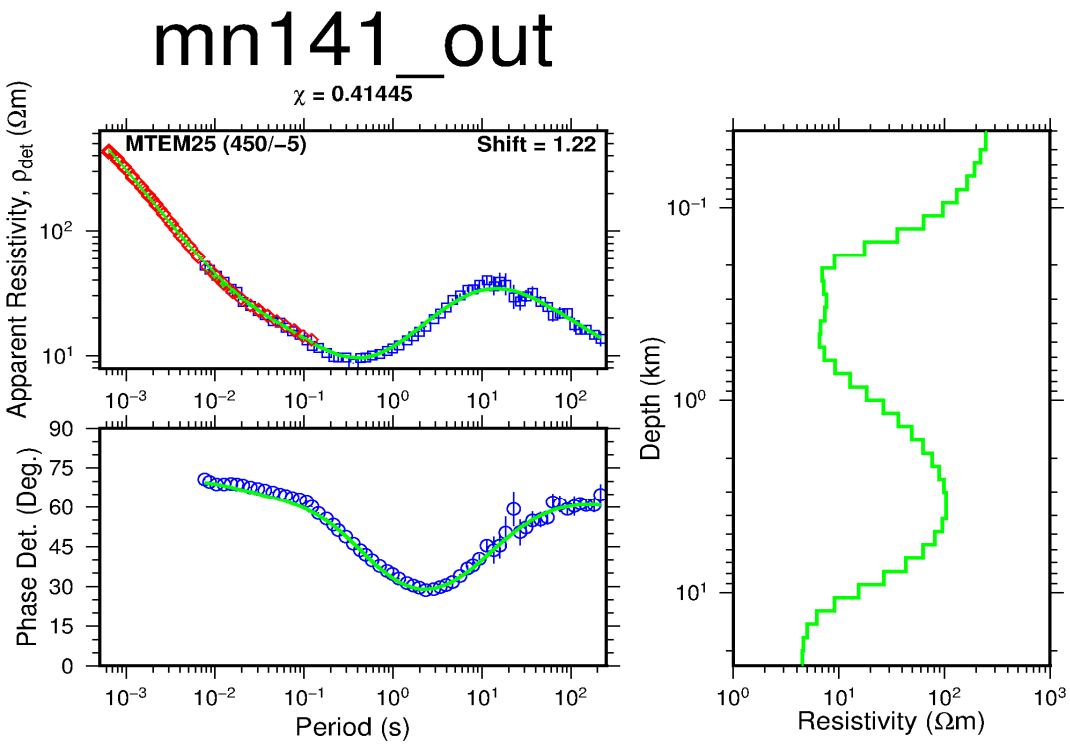

FIGURE 13: Joint 1D inversion of MT and TEM soundings

7.3 Static shift analysis

Static shift is a phenomenon in the MT method caused by local resistivity inhomogeneities which disturb the electrical field. The static shifts can be a big problem in volcanic environments where resistivity variations close to surface are often extreme. It is possible to solve the problem of static shift in the MT method through joint inversion with TEM, because TEM measurements at late time have no such distortion since they do not involve measuring the electrical field. The best static shift parameters for MT data were determined after doing joint inversion with the TEM data, then extracted from the jointly inverted models and plotted to show the spatial distribution around the prospect area. Figure 14 is a histogram of shift parameters which shows how most of the MT apparent resistivity curves were shifted down or had shifts of less than one, an indication of near surface inhomogeneities which led to galvanic distortion; 90 MT soundings were used. Figure 15 shows the spatial distribution of the shift multipliers in Menengai. The map shows that there are large areas where the MT apparent resistivity is shifted downwards while in other areas the shift is upwards.

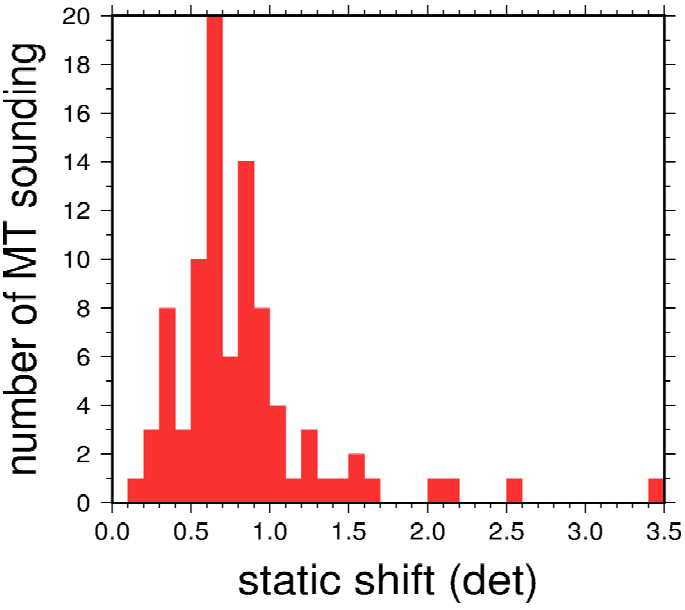

FIGURE 14: A histogram of the static shift parameters for Menengai field

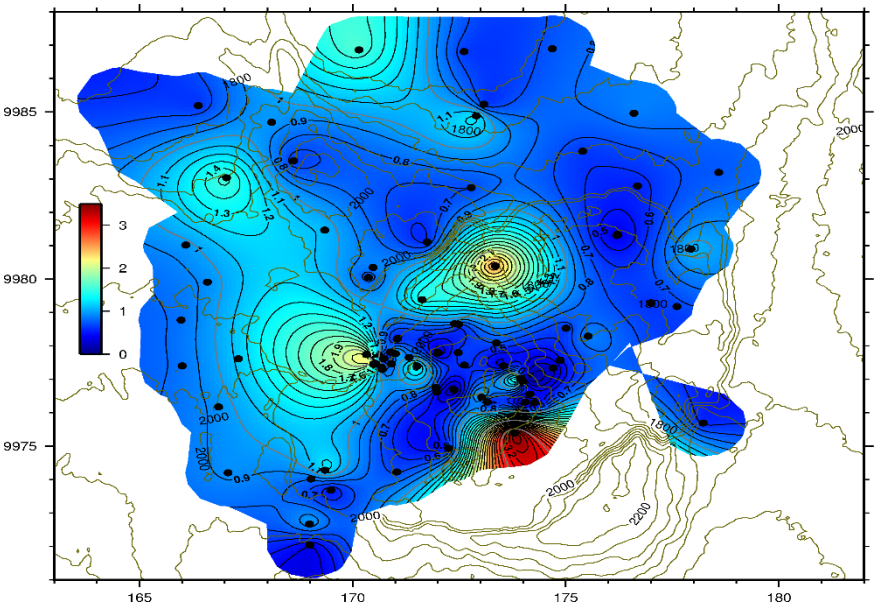

FIGURE 15: Spatial distribution of static shift parameters for determining apparent resistivity in Menengai field

7.4 Strike analysis

A rose diagram for the electrical strike direction based on the Tipper strike for periods in the range of 0.005-1 s (shallow depth) is shown in Figure 16. It gives information on dimensionality of the rock formations whereby 2D, and 3D structures could be identified. In 2D zones, the strike is more or less having the same direction, often the geological strike direction and can indicate high permeability, showing the flow path of the geothermal fluid. 3D structures can be seen as consistent alignments of the strike circling the structures. The rose diagrams on Figure 16 show no consistent alignments outside the caldera but seem to indicate a 3D structure undet the southwest part of the caldera.

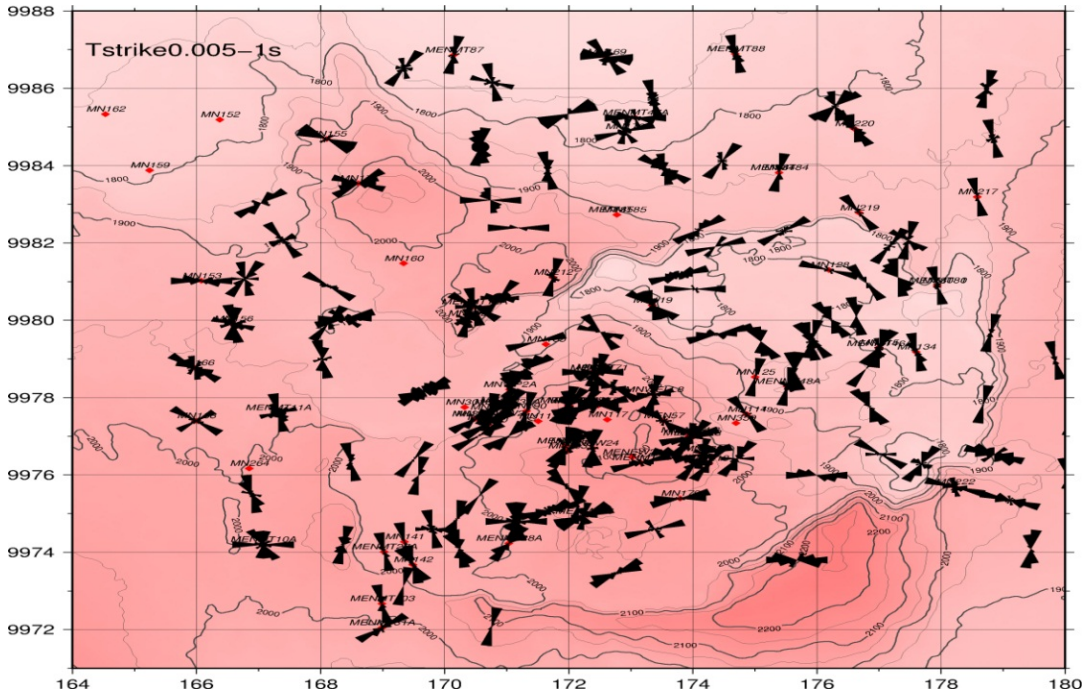

FIGURE 16: Rose diagram for the electrical strike direction based on the Tipper strike at 0.005-1 s

8. RESULTS AND DISCUSSIONS

To understand the resistivity structure of Menengai, the 1D inverted soundings were used to generate cross-sections and iso-maps. The inversion results in this report are presented in the form of selected cross-sections and iso-resistivity maps.

8.1 Cross-sections

Resistivity cross-sections were plotted from results obtained from 1D inversion by a program called TEMCROSS (Eysteinsson, 1998), developed at ÍSOR – Iceland GeoSurvey. The program calculates the best lines between the selected sites on a profile, and plots resistivity isolines based on the 1D model generated for each sounding. It is actually the logarithm of the resistivity that is contoured so the colour scale is exponential, but the numbers on the contour lines are resistivity values.

Several cross-sections were made as seen in the location map, see Figure 12. The cross-sections show a typical resistivity structure of a high-temperature field where there is a high-resistivity layer near the surface due to un-altered lava formations; underlying this resistive layer is a low-resistivity zone which is a result of low-temperature alteration minerals; this is further underlain by a high-resistivity core where chlorite and epidote usually dominate but, in Menengai, wollastonite and actinolite dominate. This gives an indication of high temperatures at increasing depth but the great temperature gradient is an indicator of another factor which, in this case, would be high-temperature hydrothermal alteration.

Cross-section NW_SE is shown in Figure 17. High resistivity from about 100 Ωm covers almost the entire surface area to a very shallow depth of about 100 m which can be associated with unaltered surface lava formations. Below the high-resistivity top layer is a low-resistivity zone with resistivity values of less than 30 Ωm; this is an indication of alteration minerals which form due to low-temperature hydrothermal activity. This low-resistivity zone extends to a depth of 1500 m from the surface. Underlying the low-resistivity zone is a high-resistive zone which seems to be lying between two conductive anomalies; this zone extends to a depth of 2500 m below the surface. However, this zone is more conspicuous in the southeast part of the profile than in the northwest. In a typical high-temperature geothermal system, this zone would coincide with the high-resistivity core where high-temperature

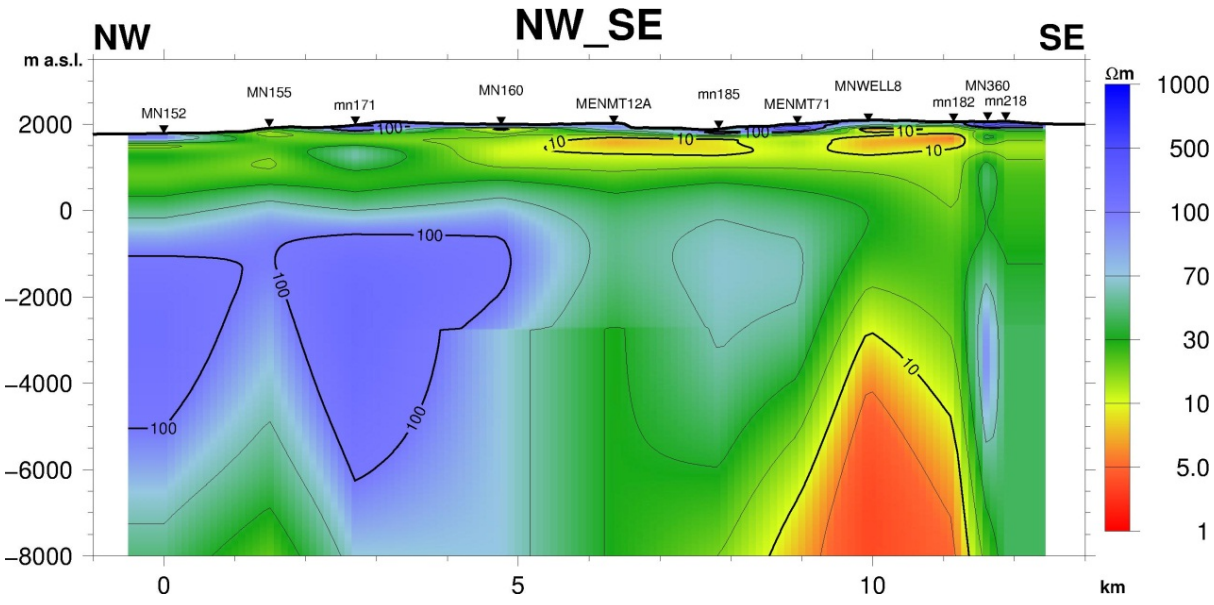

FIGURE 17: Resistivity cross-section NW_SE in Menengai field based on the output from 1D joint inversion of MT and TEM data

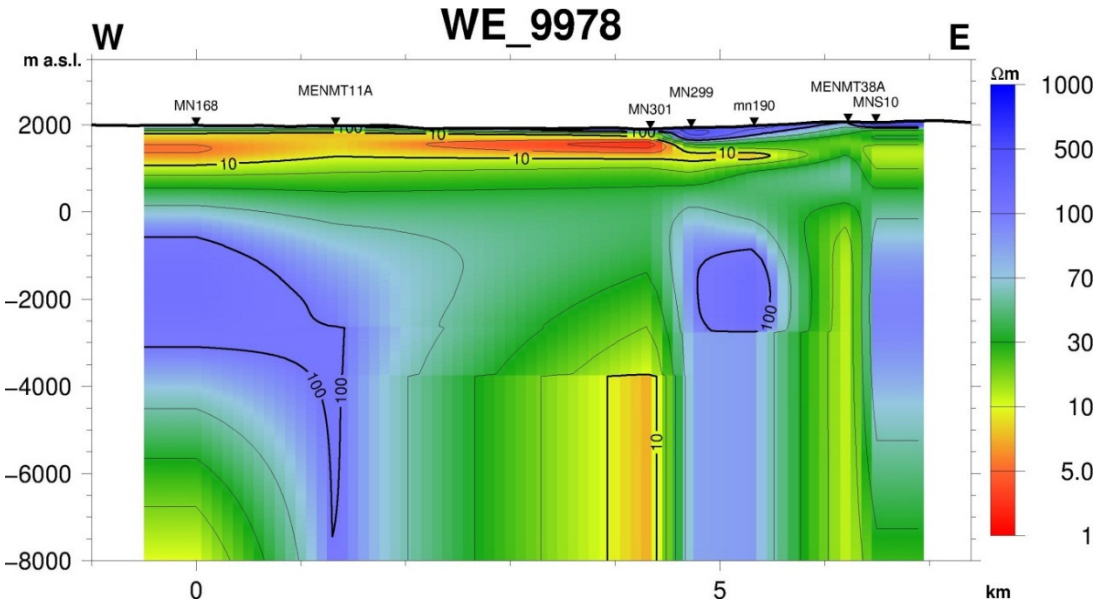

FIGURE 18: Resistivity cross-section WE_9978 in Menengai field based on the output from 1D joint inversion of MT and TEM data

hydrothermal alteration is more pronounced. Deep below this high-resistivity core is a low-resistivity anomaly with resistivity of 5 Ωm; this zone starts at a depth of 3500 m to the southeast side of the profile and is likely the heat source for the Menengai field.

Cross-section WE_9978 is shown in Figure 18. This cross-section cuts across the study area trending W-E, roughly at UTM-North 9978 km (from the South Pole). The top layer in this profile shows high resistivity of about 100 Ωm which is more pronounced in the eastern part of the profile which lies within the Menengai caldera. This is an indication of unaltered formation on the floor of the caldera. Below the high-resistivity surface is a low-resistivity anomaly with resistivity values of 10 Ωm and below and this is attributed to low-temperature hydrothermal alteration minerals. This anomalous zone extends to a depth of 1000 m below the surface. At a depth of 1500-2500 m is a high-resistivity core, which is usually associated with high-temperature hydrothermal alteration minerals in typical high-temperature, volcanically hosted, geothermal systems. At even greater depth of 4000 m below the surface is a low-resistivity anomaly with a resistivity of about 10 Ωm which could be an indication of a magma chamber or a heat source for the Menengai geothermal field.

Cross-section WE_9977 is shown in Figure 19. The section is taken across the study area trending W-E roughly at at UTM-North 9977 km (from the South Pole); and a comparison with well temperature is made. The entire surface of the profile is covered by a thin unaltered resistive layer below which is a low-resistivity anomaly with an approximate thickness of about 700 m to the west, becoming thinner as the profile tends towards the central part. However, the station coverage in the central part is poor and this could make it difficult to interpret. As we tend towards the east, the conductive anomaly becomes conspicuous and on comparing this less resistive layer with the temperature profile from a well drilled in the area, as shown in Figure 19, results indicate that this is a low-temperature alteration anomaly. Below this anomaly is a high-resistivity core which agrees with the temperature log. At a depth of 2000 m below the surface, a temperature of 388°C was recorded which correlates with the high-temperature alteration. The upper boundary of this zone can be approximated to start at a depth of 1800 m below the surface while the lower boundaries reach a depth of approximately 2500 m below the surface.

Cross-section MW-05_MW-03 is shown in Figure 20. This section cuts the study area from well MW-05 to MW-03 in a SW-NE direction. The profile covers only four soundings and the extreme southwest and northeast sections of the profile are very resistive from the surface to the bottom. However, the middle part of the profile looks promising with a low-resistivity anomaly from the surface to about 1500

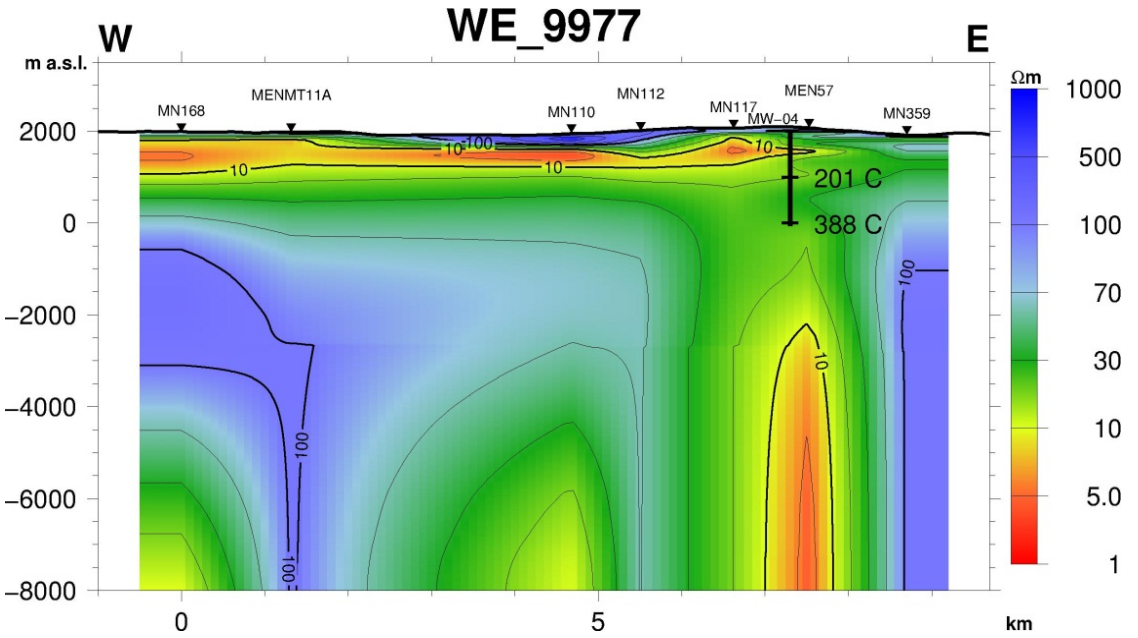

FIGURE 19: Resistivity cross-section WE_9977 in Menengai field based on the output from 1D joint inversion of MT and TEM data with a temperature profile to the east

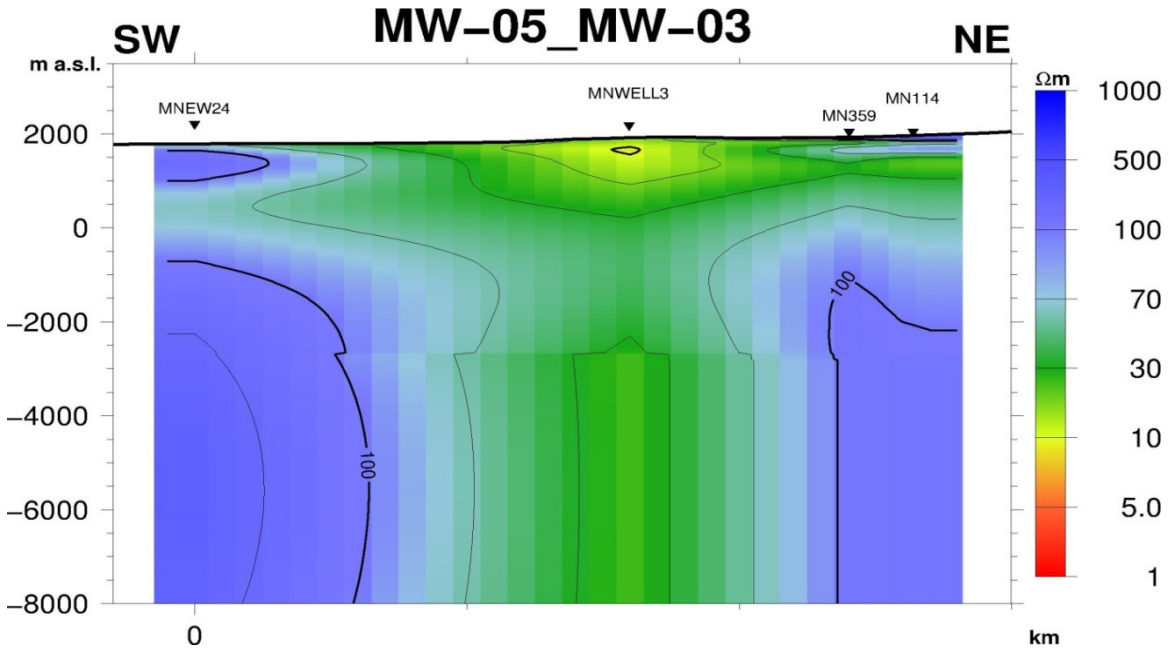

FIGURE 20: Resistivity cross-section MW-05_MW-03 in Menengai field, based on the output from 1D joint inversion of MT and TEM data

m below the surface. Below this anomaly is a high-resistivity core which extends to a depth of about 4000 m below the surface followed by a conductive body which starts from a depth of about 5000 m below the surface and extends to the bottom of the profile.

Cross-section MW-06_MS-09 is shown in Figure 21. This profile runs from MW-06_MS-09 from northwest to southeast. The surface has high resistivity which is characteristic of most unaltered rock formations. The central part of the profile has high resistivity extending from the surface to the bottom while the northwest and the southeast parts exhibit the typical resistivity structure of a high-temperature geothermal formation. This is to say that, an unaltered formation covers the surface. Thus, the resistivity

is high and below this is a conductive anomaly which overlies a high-resistivity core and below is a conductive body which has been interpreted as a possible heat source for the geothermal field.

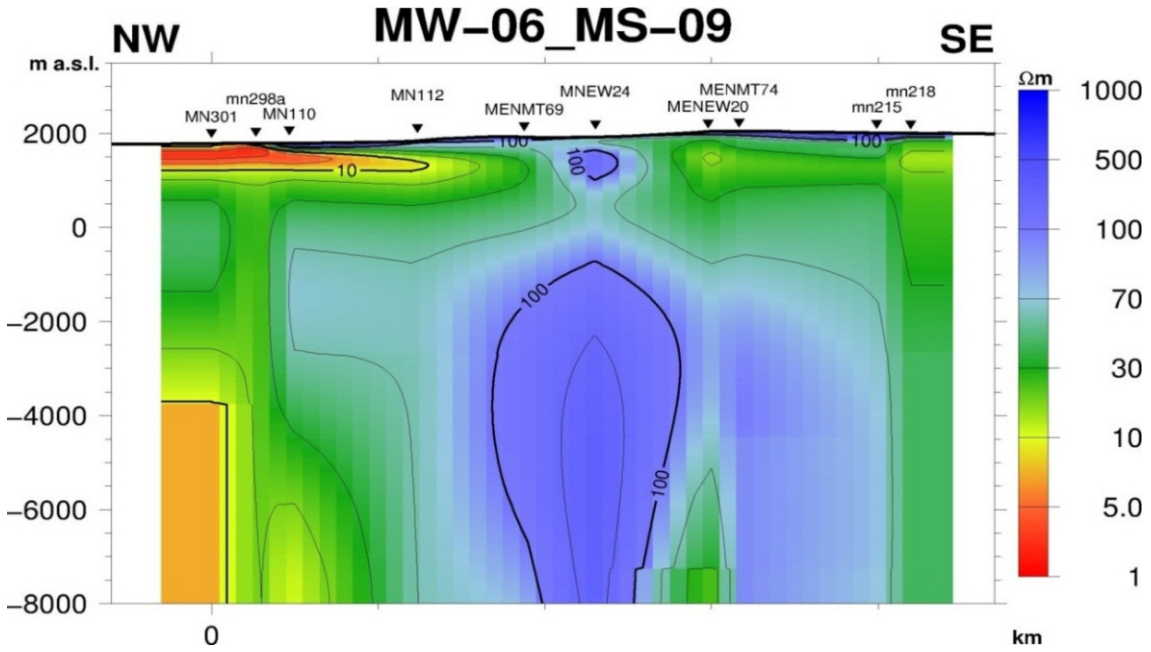

FIGURE 21: Resistivity cross-section MW-06_MS-09 in Menengai field based on the output from 1D joint inversion of MT and TEM data

8.2 Iso-resistivity maps

The programme TEMRESD developed at ÍSOR – Iceland GeoSurvey (Eysteinsson, 1998) was used to generate iso-resistivity maps at different elevations from the 1D inversion models. The resistivity is contoured and coloured in a logarithmic scale. The elevation of the Menengai field is approximately 2000 metres above sea level (m a.s.l.). In this report, iso-resistivity maps are presented from 2000 m a.s.l. to 3,000 m below sea level (m b.s.l.). As discussed earlier, in order to be able to correct for static shifts by joint inversion, a TEM sounding is needed at the same location as the MT soundings. Therefore, only the 1D jointly inverted models were used to generate the iso-resistivity maps. Only 90 MT/TEM sounding pairs, out of the 210 available MT soundings and over 150 TEM soundings, fulfilled this critera and were considered.

Resistivity map at 2000 m a.s.l. is shown in Figure 22 and is a representation of the surface level. The sounding distribution in this map is not good because many of the sounding sites are at lower altitude. However, it is noted that the surface is covered entirely by highly resistive lavas which explains why the resistivity is greater than 56 Ωm for the entire area.

Resistivity map at 1500 m a.s.l. is shown in Figure 23. This map is about 500 m below the surface and shows a low-resistivity anomaly covering the entire study area. The low-resistivity anomaly at this level is believed to be a result of low-temperature alteration minerals. The resisitivity at this altitude is about 5 Ωm in the most conductive southern part and 30 Ωm in the most resistive northern part and the area inside the caldera.

Resistivity map at 1000 m a.s.l. is shown in Figure 24. This is approximately 1000 m below the surface and the resistivity at this zone is relatively low. The resistivity of the entire study area at this depth is about 40 Ωm which is an increase compared to the resistivity at 1500 m a.s.l. This increase in resistivity could be a reflection of a possible transition from low-temperature alteration minerals to high-temperature alteration minerals.

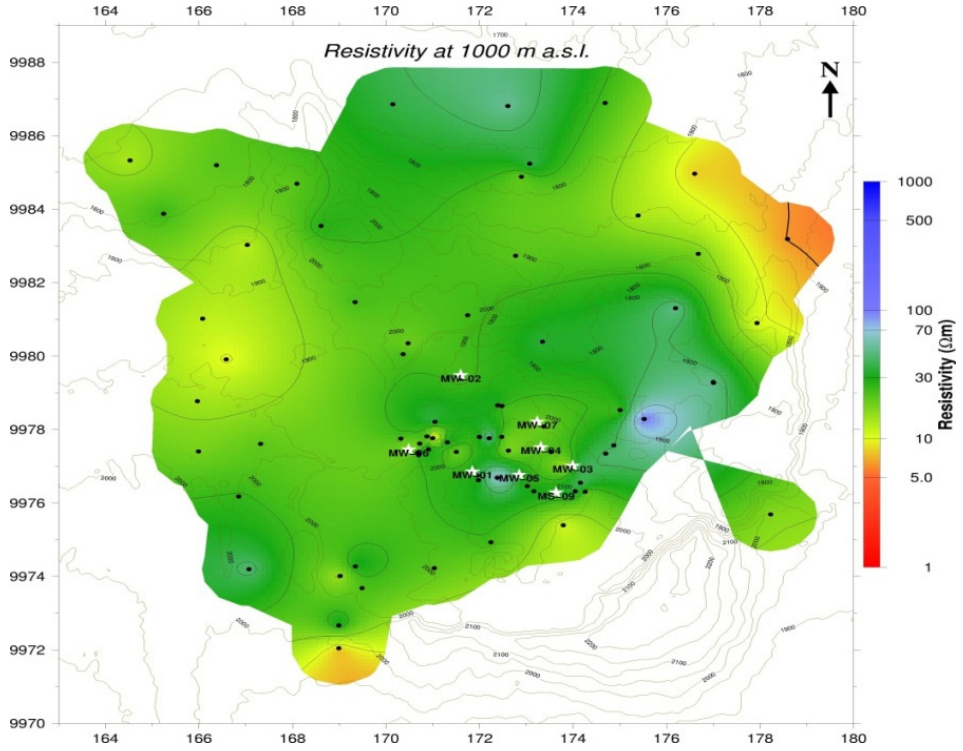

FIGURE 24: Iso-resistivity map in Menengai field at 1000 m a.s.l; black dots denote 1D inversion models while the white stars represent Menengai wells

Resistivity map at 0 m a.s.l. is shown in Figure 25. This iso-resistivity map at sea level shows an increase in resistivity as compared to Figures 23 and 24. A high-resistivity core of about 30 Ωm in the southern part of the study area is evident, and could be interpreted as an indication of high-temperature alteration minerals, in which case the zone would mark the core of the reservoir for the Menengai geothermal field. All the other parts at this depth are covered by a high-resistivity formation with resistivity greater than 100 Ωm.

Resistivity map at 1000 m b.s.l. is shown in Figure 26. This map shows resistivity at a depth of about 3000 m below the surface and the resistivity structure of the study area at this point resembles the resistivity structure at sea level. This gives a possibility of the high-resistivity core extending to this depth; thus, the thick resistivity core would be an indication of a good reservoir for a high-temperature system.

Resistivity map at 2000 m b.s.l is shown in Figure 27. At a depth of approximately 4000 m below the surface, the resistivity decreases further in the southern part of the study area to lows of 5 Ωm, giving an indication of a possible heat source. If indeed this is the heat source, then it must be the source of heat to the possible reservoir zone at a depth of between 400 m b.s.l. and 1000 m b.s.l. The rest of the study area is highly resistive at this depth.

Resistivity map at 3000 m b.s.l. is shown in Figure 28. This further confirms the possibility of a heat source beneath the Menengai caldera with decreasing resistivity. The resistivity within the caldera at this point is less than 5 Ωm.

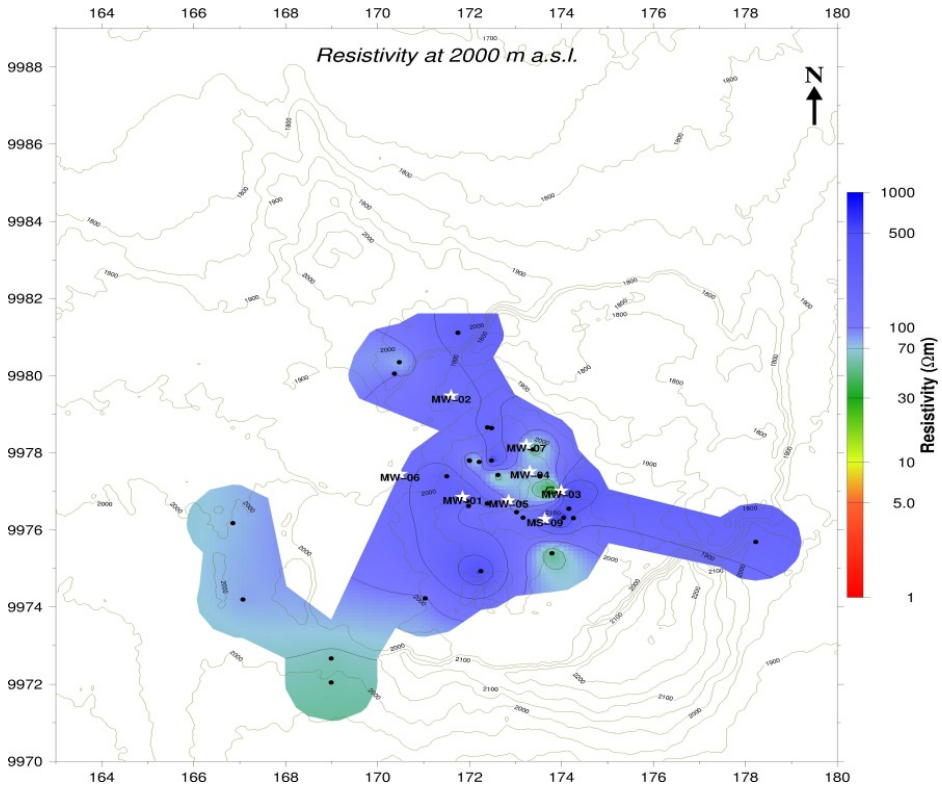

FIGURE 22: Iso-resistivity map in Menengai field at 2000 m a.s.l; black dots denote 1D inversion models while the green (grey) stars represent Menengai wells

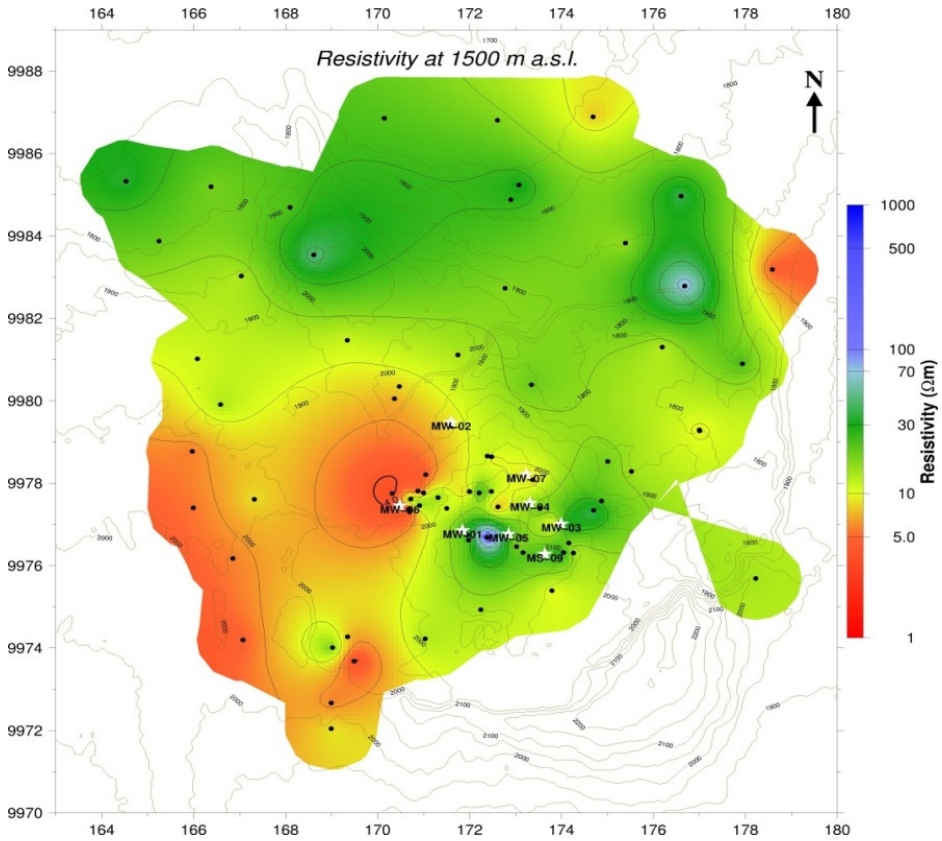

FIGURE 23: Iso-resistivity map in Menengai field at 1500 m a.s.l; black dots denote 1D inversion models while the white stars represent Menengai wells

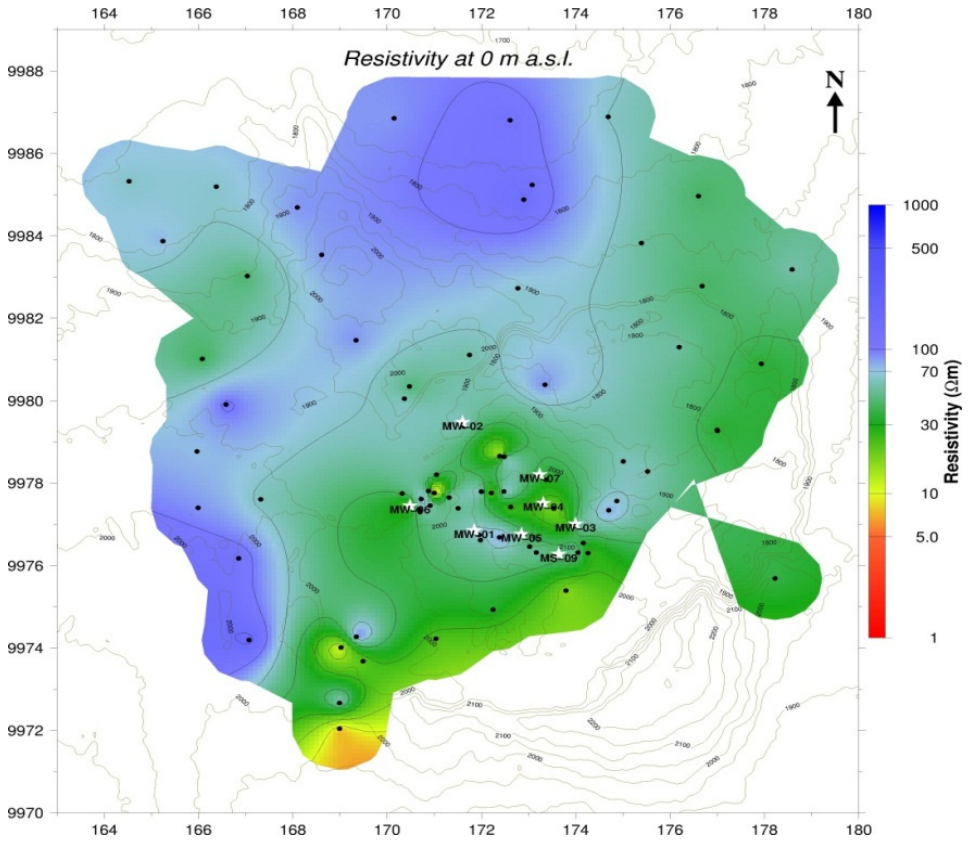

FIGURE 25: Iso-resistivity map in Menengai field at sea-level; black dots denote 1D inversion models while the white stars represent Menengai wells

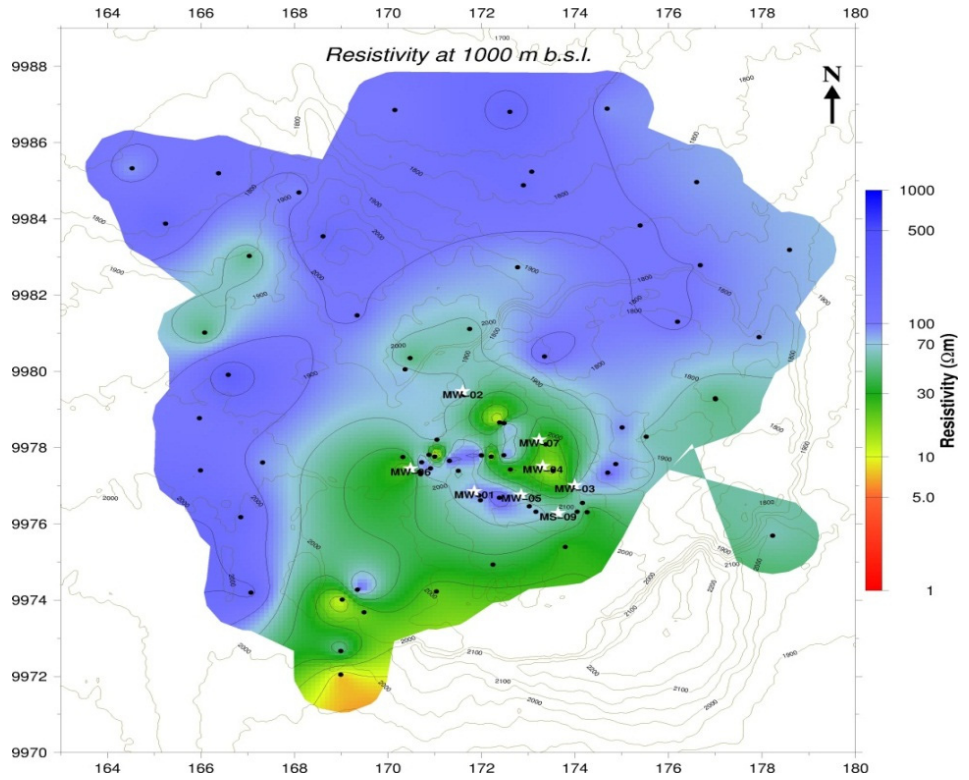

FIGURE 26: Iso-resistivity map in Menengai field at 1000 m b.s.l; black dots denote 1D inversion models while the white stars represent Menengai wells

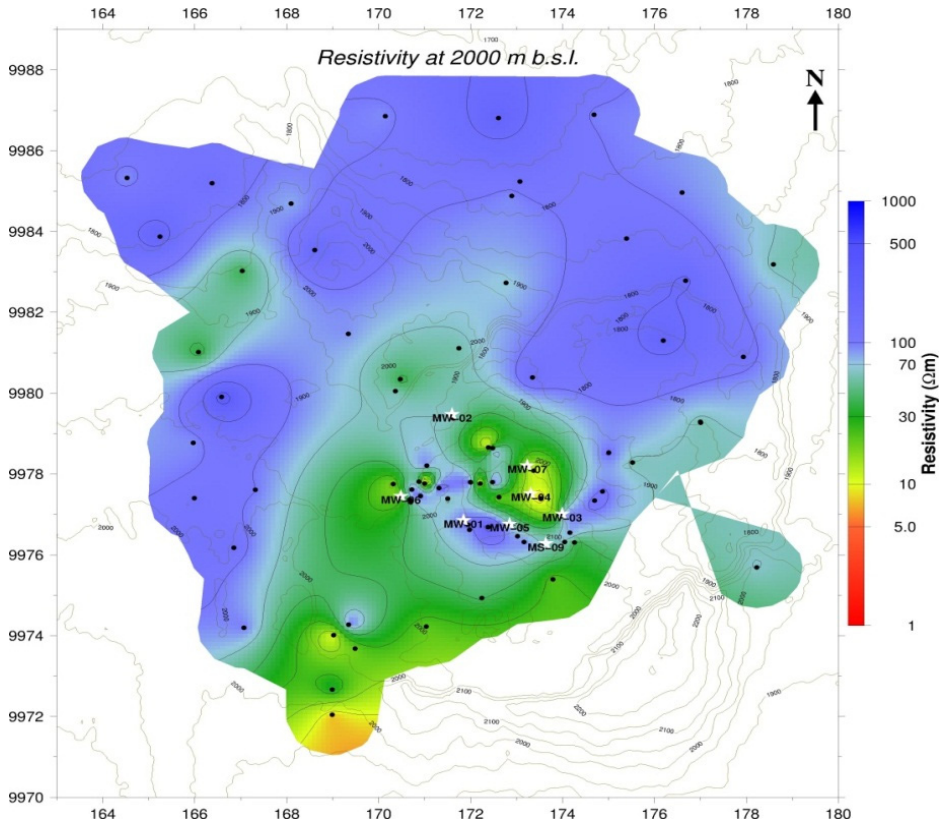

FIGURE 27: Iso-resistivity map in Menengai field at 2000 m b.s.l.; black dots denote 1D inversion models while the white stars represent Menengai wells

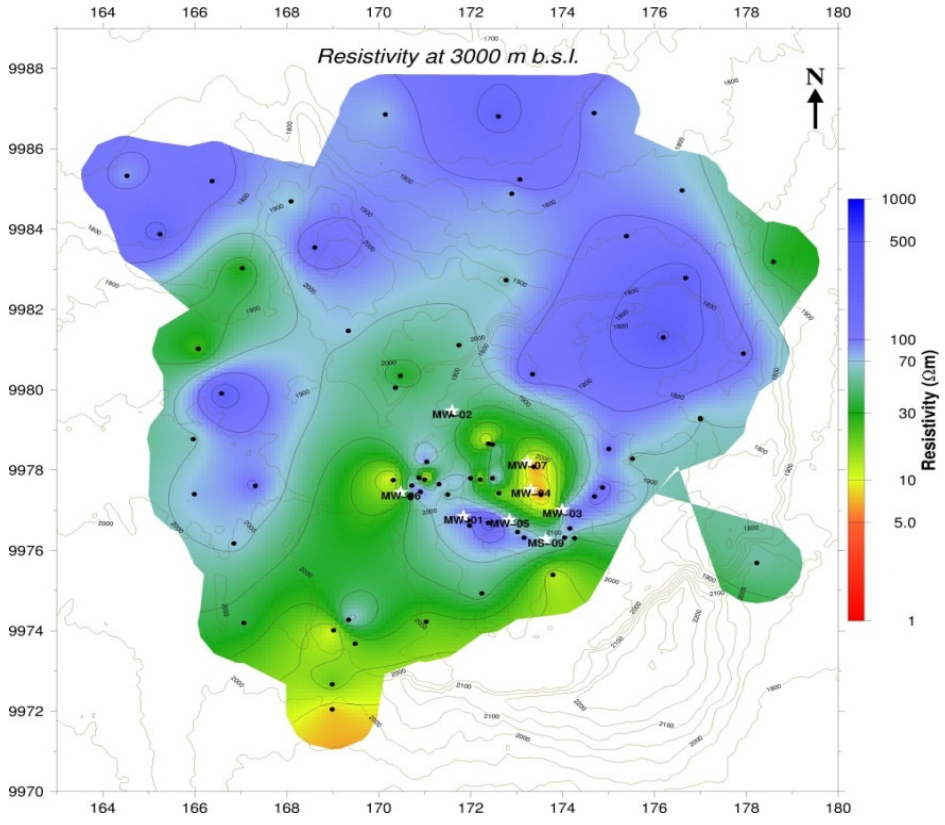

FIGURE 28: Iso-resistivity map in Menengai field at 3000 m b.s.l; black dots denote 1D inversion models while the white stars represent Menengai wells

8.3 Comparison of resistivity with temperature in Menengai field

Temperature measured in well MW-04 (refer to Figure 19) tends to agree with the resistivity structure of Menengai. At a depth of 1000 m below the surface, the resistivity structure of Menengai, as seen in this cross-section, shows a low-resistivity anomaly which is interpreted to be the cap-rock and whose resistivity could be reflecting the low-temperature alteration minerals. A temperature of 201°C was measured at this depth.

Temperature measured at a depth of 2000 m in the well also agrees with the resistivity at that depth because high-temperature hydrothermal alteration minerals like chlorites and epidotes are know to exhibit high resistivity due to their crystalline nature. Therefore, the measured temperature of 388°C is a good indication, and probably a confirmation, of the existence of high-temperature minerals in Menengai field at depths between 1600 and 3000 m below the surface; this could be used to mark the upper and lower boundaries of the reservoir zone in Menengai geothermal field.

From this comparison, it is most likely that the low-resistivity anomaly zone below the high-resistivity core would be the heat source and extremely high temperatures would be expected there.

9. CONCLUSIONS AND RECOMMENDATIONS

From the results of the joint inversion of MT and TEM data, the following resistivity layers exist as seen in the cross-sections:

- A thin shallow high-resistivity layer at the surface and near the surface with resistivity, >100 Ωm is observed and is interpreted to be a layer of un-altered formations about 300 m thick; the conduction mechanism is pore fluid conduction.
- This is followed by a 700 m thick low-resistivity layer, < 10 Ωm which is believed to be a result of low-temperature hydrothermal alteration minerals such as zeolites; the conduction mechanism in this zone is mainly mineral conduction.
- A relatively higher-resistivity zone follows with resistivity ranging between 30 and 60 Ωm where the resistivity is dominated by resistive high-temperature alteration minerals such as wollastonite, chlorite and epidote. This layer would define the reservoir zone in a typical high-temperature volcanically hosted geothermal system and, thus, it is believed that it could be the reservoir zone for Menengai field. The depth of this zone within the caldera is approximately between 1600 and 3000 m below the surface.
- A low-resistivity anomaly which was interpreted to be a deep conductor was seen at 4000 m below the surface and has been postulated to be associated with the heat source. If this deep conductor is a heat source, then Menengai hosts a relatively shallow heat source.

There seems to be a fairly good correlation between resistivity and measured temperature, as evidenced from well MW-04.

It is recommended that more TEM data be collected at the same sites as the MT locations in order to correct for the static shift in the MT soundings. This would greatly help in refining the results currently discussed in this report because better coverage would improving the resistivity image of the field.

It is also recommended that an efford is done to correlate the resistivity structure with alteration mineralogy as observed in wells. This would help in understanding the field in greater detail and, given that Menengai has now several wells, this would be an easy task and would give enomous information, especially in delineating the resource area and the depths of each zone, namely: the caprock, the reservoir and the heat source.

ACKNOWLEDGEMENTS

I would like to express my sincere gratitude to the UNU-GTP and the Government of Iceland for awarding me this scholarship to participate in the six month training programme. Many thanks go to Dr. Ingvar Birgir Fridleifsson, the director, Mr. Lúdvík S. Georgsson, the deputy director, Ms. Thórhildur Ísberg, Mr. Ingimar G. Haraldsson, Ms. Málfrídur Ómarsdóttir and Mr. Markús A.G. Wilde, and all of UNU staff for their coordination of the training activities and for being available to give guidance and help whenever I needed it. I am sincerely grateful to you all.

For my supervisors: Mr. Knútur Árnason and Mr. Gylfi Páll Hersir you were always there whenever I needed your guidance from the time of specialised training to the time of this research work. And Andemariam Teklesenbet Beyene, you took us through the most critical stage of our research by coming to the study room daily to take us through data processing: much appreciation.

Special thanks go to Charles Muturia Lichoro for his assistance in handling my research data, too much for me to handle singlehandedly. I am grateful to my employer, the Geothermal Development Company Ltd. – GDC, for providing the data used in this study and for granting me leave to undertake this course. Special thanks to my colleagues at the geophysics office for their support through data collection - I thank you so much for your support. To all the 2012 UNU Fellows, I say thank you very much for the wonderful time and discussions that we shared together. To my beloved family, your patience in waiting to see me again, your love and prayers throughout my stay here in Iceland were very encouraging and gave me more strength to carry on. May God bless all of you.

REFERENCES

Archie, G.E., 1942: The electrical resistivity log as an aid in determining some reservoir characteristics. *Tran. AIME, 146,* 54-67.

Árnason, K., 1989: *Central-loop transient electromagnetic sounding over a horizontally layered earth*. Orkustofnun, Reykjavík, report OS-89032/JHD-06, 129 pp.

Árnason, K., 2006a: *TemX Short manual*. ÍSOR – Iceland GeoSurvey, Reykjavík, manual, 17 pp.

Árnason, K., 2006b: *TEMTD, a program for 1D inversion of central-loop TEM and MT data. Short manual*. ÍSOR – Iceland GeoSurvey, Reykjavík, manual, 17 pp.

Árnason, K., Karlsdóttir, R., Eysteinsson, H., Flóvenz, Ó.G., and Gudlaugsson, S.Th., 2000: The resistivity structure of high-temperature geothermal systems in Iceland. *Proceedings of the World Geothermal Congress 2000*, *Kyushu-Tohoku, Japan,* 923-928.

Berdichevsky, M.N., and Dmitriev, V.I., 2002: *Magnetotellurics in the context of the theory of ill posed problems.* Society of Exploration Geophysicists, USA, 215 pp.

Berktold, A., 1983: Electromagnetic studies in geothermal regions. *Geophysical Surveys, 6*, 173-200.

Christensen, A., Auken, E., and Sørensen, K., 2006: The transient electromagnetic method. *Groundwater Geophysics, 71*, 179-225.

Dakhnov, V.N., 1962: Geophysical well logging. *Q. Colorado Sch. Mines, 57-2*, 445 pp.

Encyclopaedia Britannica, 2010: *Solar wind*. Encyclopaedia Britannica, online, webpage: *www.britannica.com/EBchecked/topic/1589681/Solar-Dynamics-Observatory.*

Eysteinsson, H., 1998: *TEMMAP and TEMCROSS plotting programs*. ÍSOR – Iceland GeoSurvey, unpublished programs and manuals.

Flóvenz, Ó.G., Georgsson, L.S., and Árnason, K., 1985: Resistivity structure of the upper crust in Iceland, *J. Geophys. Res., 90-B12*, 10,136-10,150.

Flóvenz, Ó.G., Spangenberg, E., Kulenkampff, J., Árnason, K., Karlsdóttir, R., and Huenges E., 2005: The role of electrical conduction in geothermal exploration. *Proceedings of the World Geothermal Congress 2005, Antalya, Turkey,* CD, 9 pp.

Flóvenz, Ó.G., Hersir, G.P., Saemundsson, K., Ármannsson, H., and Fridriksson, Th., 2012: Geothermal energy exploration techniques. In: Syigh, A. (ed.), *Comprehensive Renewable Energy, Volume 7*, Elsevier, Oxford, 51-95.

GDC, 2010: *Menengai geothermal prospect, an investigation for its geothermal potential.* GDC, Kenya, Geothermal resource assessment project, unpubl. report.

Geotermica Italiana, 1987: *Geothermal reconnaissance survey in the Menengai-Bogoria area of the Kenya Rift Valley.* UN/DTC report.

Gichira, J.M., 2012: *Appendix I to the report "Joint 1D inversion of MT and TEM data from Menengai geothermal field, Kenya."* UNU-GTP, Iceland, report 11 appendix I, 47 pp.

Hermance, J.F., 1973: Processing of magnetotelluric data. *Earth and Planetary Interiors, 7*, 349-364.

Hersir, G.P., and Björnsson, A., 1991: *Geophysical exploration for geothermal resources. Principles and applications*. UNU-GTP, Iceland, report 15, 94 pp.

Keary, P., Brooks, M., and Hill, I., 2002: *An introduction to geophysical exploration.* Blackwell Scientific Publications, Oxford, 262 pp.

Keller, G.V., and Frischknecht, F.C., 1966: *Electrical methods in geophysical prospecting*. Pergamon Press Ltd., Oxford, 527 pp.

Lichoro, C.M., 2009: Joint 1-D inversion of TEM and MT data from Olkaria Domes geothermal area, Kenya. Report 16 in: *Geothermal training in Iceland 2009*. UNU-GTP, Iceland, 289-318.

Lee Lerner, K., Lerner, B.W., and Cengage, G., 2006: *Porosity and permeability.* World of Earth Science, webpage*: www.enotes.com/earth-science/.*

Simiyu, S.M., Oduong, E.O., and Mboya, T.K., 1998: *Shear wave attenuation beneath the Olkaria volcanic field*. KenGen, Kenya, internal report.

Sternberg, B.K., Washburne, J.C., and Pellerin, L., 1988: Correction for static shift in magnetotellurics using transient electromagnetic soundings. *Geophysics, 53*, 1459-1468.